nature cell biology

Kinetochore kinesin CENP-E is a processive bi-directional tracker of dynamic microtubule tips

Nikita Gudimchuk[1,5], Benjamin Vitre[2,5], Yumi Kim[2,6], Anatoly Kiyatkin[1], Don W. Cleveland[2], Fazly I. Ataullakhanov[3,4] and Ekaterina L. Grishchuk[1,7]

During vertebrate mitosis, the centromere-associated kinesin CENP-E (centromere protein E) transports misaligned chromosomes to the plus ends of spindle microtubules. Subsequently, the kinetochores that form at the centromeres establish stable associations with microtubule ends, which assemble and disassemble dynamically. Here we provide evidence that after chromosomes have congressed and bi-oriented, the CENP-E motor continues to play an active role at kinetochores, enhancing their links with dynamic microtubule ends. Using a combination of single-molecule approaches and laser trapping *in vitro*, we demonstrate that once reaching microtubule ends, CENP-E converts from a lateral transporter into a microtubule tip-tracker that maintains association with both assembling and disassembling microtubule tips. Computational modelling of this behaviour supports our proposal that CENP-E tip-tracks bi-directionally through a tethered motor mechanism, which relies on both the motor and tail domains of CENP-E. Our results provide a molecular framework for the contribution of CENP-E to the stability of attachments between kinetochores and dynamic microtubule ends.

Accurate chromosome segregation depends on interactions between microtubules and the kinetochore, a protein structure localized at each centromere[1]. Initially, kinetochores often attach to the walls of microtubules with the chromosomes then moving towards a spindle pole in a dynein-dependent manner[2,3]. The pole-proximal chromosomes then need to congress, that is, move to the spindle midzone where microtubule plus ends are located. The centromere protein CENP-E, a microtubule-dependent plus-end-directed motor of the kinesin-7 subfamily, is essential for congression of initially misaligned chromosomes[4–8]. Perturbation of CENP-E function using antibody injection[9] or depletion[10], gene inactivation[11], short interfering RNA (siRNA) depletion[12], or inhibition with a small-molecule inhibitor[13] blocks microtubule plus-end-directed motion of pole-proximal chromosomes, accompanied by a failure of both kinetochores to form stable microtubule attachments[11].

Previous work has suggested that the role of CENP-E in mitosis is not limited to the transport of chromosomes during congression. First, CENP-E is detected at the kinetochores of already congressed chromosomes[14,15]. Second, depletion of CENP-E induces up to a 50% reduction in the number of microtubules on congressed chromosomes[11,16]. Third, CENP-E gene deletion leads to an increased proportion of lagging chromosomes in anaphase in mouse liver cells and embryonic fibroblasts[11,17]. Fourth, after CENP-E-mediated congression, CENP-E-dependent localization of protein phosphatase 1 (PP1) to kinetochores is still required for stable microtubule capture by those kinetochores[8]. Furthermore, antibodies against CENP-E block the motions of isolated mammalian chromosomes at the ends of depolymerizing microtubules *in vitro*[18]. Despite these observations, whether CENP-E plays a physiological role at the kinetochore–microtubule interface of congressed chromosomes and the possible underlying molecular mechanisms for these findings remain controversial.

Mechanochemical enzymes such as kinesins transport intracellular cargos by walking along microtubule tracks. The well-studied kinesin-1, a plus-end-directed motor, carries axonal organelles towards microtubule ends, where the motor dissociates from the microtubule and unloads its cargo[19]. However, the chromosomal cargo carried by CENP-E kinesin is unusual; after the kinetochore has encountered the ends of the microtubule tracks, it does not detach but remains stably associated with the tips of microtubules (refs 20,21). The nature of the connections that link the kinetochores of congressed chromosomes and microtubule ends is not well understood, but these links are known to

[1]Physiology Department, Perelman School of Medicine, University of Pennsylvania, Philadelphia, Pennsylvania 19104, USA. [2]Ludwig Institute for Cancer Research and Department of Cellular and Molecular Medicine, University of California, San Diego, La Jolla, California 92093, USA. [3]Center for Theoretical Problems of Physicochemical Pharmacology, Russian Academy of Sciences, Moscow 119991, Russian Federation. [4]Federal Research and Clinical Centre of Pediatric Hematology, Oncology and Immunology, Moscow 117513, Russian Federation. [5]These authors contributed equally to this work. [6]Present address: Department of Molecular and Cell Biology, University of California, Berkeley, California 94704, USA.
[7]Correspondence should be addressed to E.L.G. (e-mail: gekate@mail.med.upenn.edu)

Received 16 January 2013; accepted 22 July 2013; published online 18 August 2013; DOI: 10.1038/ncb2831

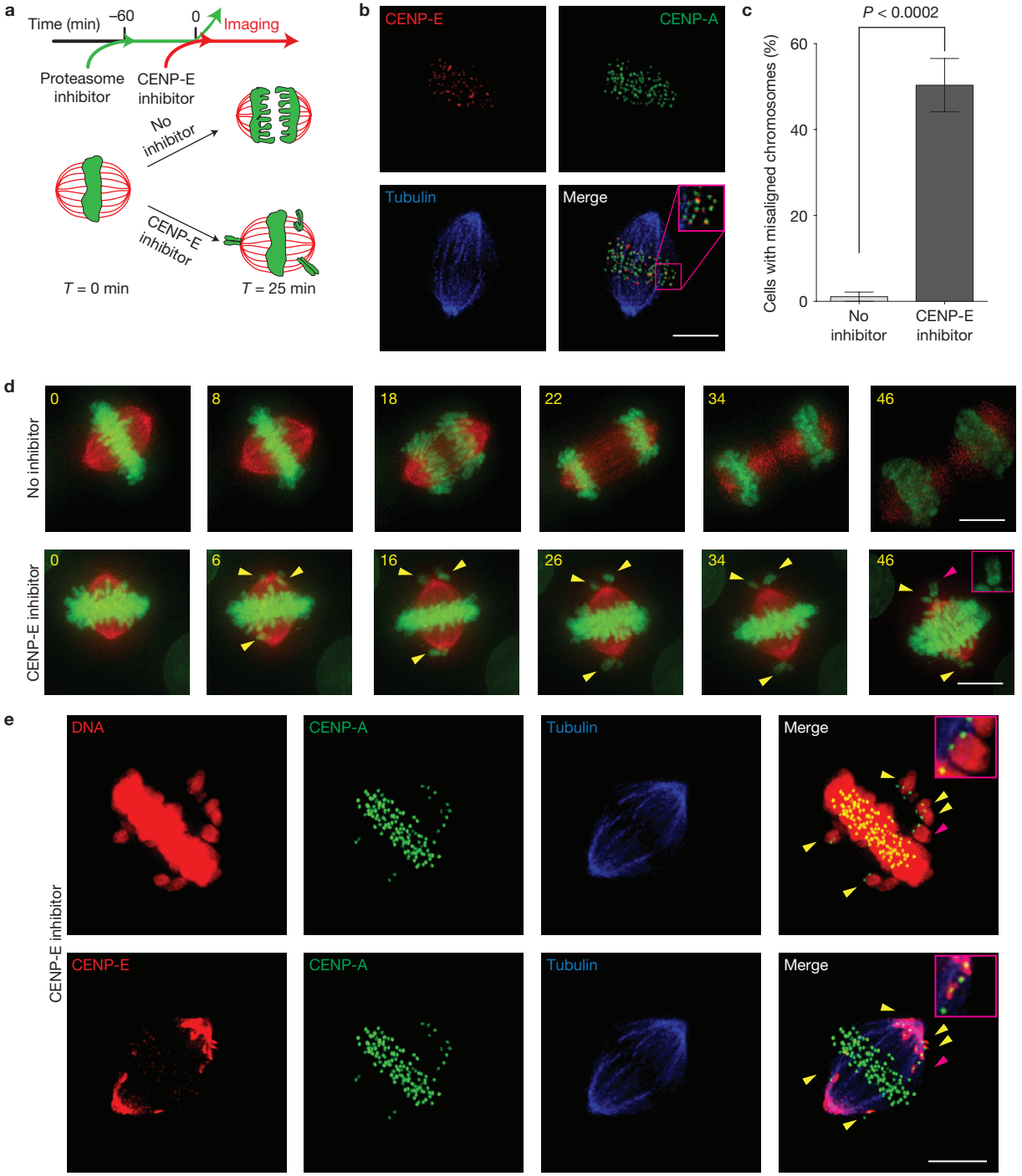

Figure 1 Loss of chromosome alignment in metaphase cells with inhibited CENP-E kinesin. (**a**) Schematic diagram of the assay with metaphase-arrested HeLa cells. (**b**) Immunostaining of a HeLa cell arrested at metaphase with the proteasome inhibitor Velcade; CENP-A is a centromere and kinetochore marker. (**c**) Percentage of cells in which at least one chromosome lost its alignment (mean±s.e.m.); based on $n=3$ independent experiments (50 cells in total) for the no inhibitor condition and $n=4$ independent experiments (70 cells in total) for the CENP-E inhibitor condition. A two-tailed unpaired *t*-test indicates a significant difference between these results. (**d**) Time-lapse images of HeLa cells treated with Velcade for 1 h, and then released into medium containing DMSO or GSK-923295 (Supplementary Video S1). The numbers are minutes after Velcade washout. The arrows point to chromosomes that lost alignment (yellow) or that are enlarged in the inset (pink). (**e**) Immunofluorescence images of a HeLa cell released from Velcade into CENP-E inhibitor for 15 min and stained for DNA, CENP-A, CENP-E and tubulin; three-colour overlays are shown in each row. Scale bars, 5 μm.

permit exchange of tubulin dimers at the microtubule ends, implying that each kinetochore can processively track dynamic microtubule ends[20,22]. This is a remarkable property because the kinetochore maintains its attachment to the site where tubulin dimers are being added or lost on the microtubule polymer. Only two proteins that exhibit bi-directional tip-tacking *in vitro* have thus been identified[23–25].

Here we examine whether the CENP-E kinesin can facilitate end-on microtubule attachments.

RESULTS

The CENP-E motor acts at kinetochores of congressed chromosomes

To investigate a possible contribution of CENP-E to linking microtubule plus ends to the kinetochores on congressed chromosomes we used a specific small-molecule inhibitor GSK-923295, which locks CENP-E in a rigor microtubule-bound state[13]. HeLa cells were arrested in metaphase with a proteasome inhibitor, which was then replaced with the CENP-E inhibitor or dimethylsulphoxide (DMSO) as a control (Fig. 1a). In control metaphase cells, CENP-E was clearly visible at the kinetochores (Fig. 1b); chromosome alignment was maintained in all but 1 out of 50 cells and anaphase started ~30 min after removing the proteasome inhibitor (Fig. 1c,d). Addition of GSK-923295 to metaphase cells caused a marked depletion of the kinetochore-localized CENP-E (Fig. 1e), probably due to the passive transport of the rigor bound motor by poleward microtubule flux[6]. Importantly, in ~50% of CENP-E-inhibited cells there was a clear loss of chromosome alignment (3.6 chromosome pairs per cell). One of the sister kinetochores on such pairs seemed to assume microtubule-lateral binding, and moved towards the pole (Fig. 1e, lower inset). Subsequently, these chromosomes accumulated at the poles and anaphase was delayed (Supplementary Video S1), the hallmark features of the loss of CENP-E function[9,11,17]. These results clearly demonstrate that CENP-E contributes not only to the congression of pole-proximal chromosomes[5,7], but it also continues to be motor active at the kinetochores of congressed chromosomes.

Single molecules of full-length and truncated CENP-E walk similarly along microtubule walls

The above finding prompted us to reconstitute CENP-E interactions with microtubules *in vitro* using purified proteins. To examine transport properties of the previously uncharacterized wild-type version of CENP-E, hereafter called full-length CENP-E, we used total internal reflection fluorescence (TIRF) microscopy to visualize a carboxy-terminal fusion of it to GFP (Fig. 2a,b). Many encounters between single full-length molecules and coverslip-attached, Taxol-stabilized microtubules led to short-lived diffusive motions, suggesting auto-inhibition of soluble full-length CENP-E (refs 26,27; Fig. 2c and Supplementary Fig. S1a–d). However, some full-length molecules in our preparations lacked such inhibition and moved unidirectionally and processively, similar to a truncated CENP-E, in which the motor domains were dimerized with a shortened coiled-coil stalk[6,28] (Fig. 2a). These proteins were then conjugated by their C termini to 0.5 μm beads, and laser tweezers were used to launch these beads on microtubule walls (Supplementary Fig. S1e–g and Video S2). A significantly larger fraction of processive motions was observed with beads coated with full-length CENP-E versus what was seen with the soluble bead-free molecules (Supplementary Fig. S1h), suggesting that conjugating the tail of full-length CENP-E to a bead cargo partially relieves the auto-inhibition, as in kinesin-1 (ref. 29). Detailed quantification of the single-molecule and bead motility in these assays revealed that the microtubule wall-dependent transport by the full-length motor is highly similar to that of truncated CENP-E (Supplementary Table S1; refs 8,28,30).

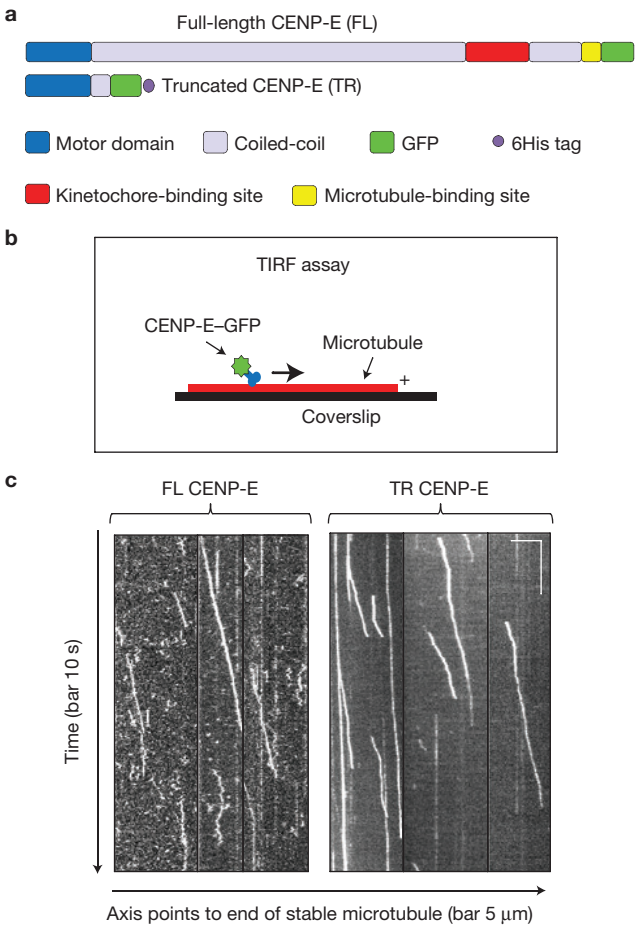

Figure 2 Motility of single molecules of CENP-E on microtubule wall. (**a**) Domain structure of the *Xenopus laevis* CENP-E proteins used for *in vitro* experiments. These drawings are not to scale; full-length (FL) CENP-E is almost 230 nm long[6], but both proteins have C-terminal GFP fusions. (**b**) Schematic diagram of the TIRF assay with stable microtubules. (**c**) Typical kymographs of single-molecule motions. Fewer full-length CENP-E molecules show processive plus-end-directed walking, but these motions are quantitatively similar to the walking of the truncated (TR) CENP-E motor.

Single molecules of full-length but not truncated CENP-E can processively track dynamic microtubule ends

We then analysed what happens when CENP-E walks to the ends of microtubule tracks. On reaching the plus tips of stable microtubules, both full-length and truncated CENP-E constructs paused at the tip for 2–4 s before detaching[8], significantly longer than 0.3 ± 0.1 s (mean ± s.e.m., $n = 253$) for kinesin-1 studied under identical conditions (Supplementary Fig. S2a and Table S2). This finding may explain an increase in the rate of microtubule polymerization, which was observed previously with human truncated CENP-E motor in the presence of Taxol[31]. To examine how CENP-E interacts with the physiologically relevant, dynamic microtubule ends, we grew non-stabilized polymers from coverslip-attached microtubule seeds (Fig. 3a). Both full-length and truncated CENP-E proteins walked fast enough to catch up with the growing microtubule end. Interestingly, the truncated molecules detached from these ends more rapidly than from

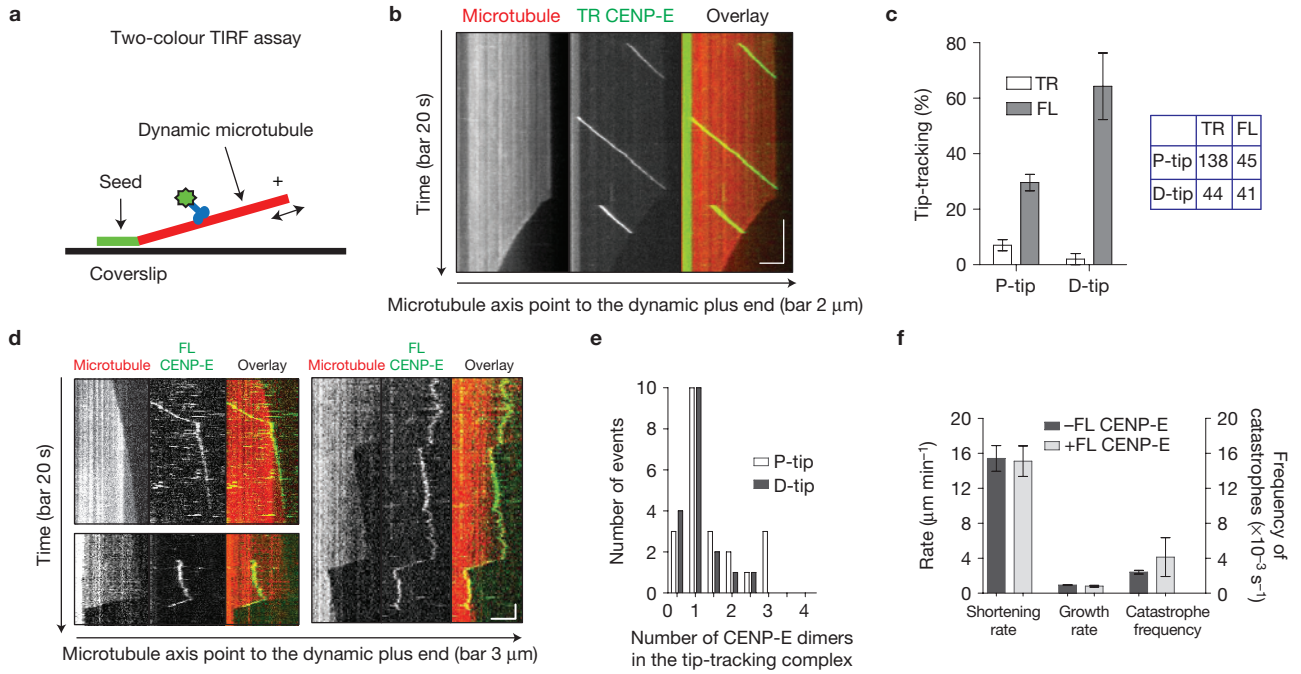

Figure 3 Single molecules of CENP-E visualized at dynamic microtubule tips. (**a**) Schematic of a single-molecule assay with dynamic microtubules. (**b**) Kymographs of walking truncated CENP-E molecules, which fall off the growing, then shrinking, microtubule tip. (**c**) Percentage of complexes tracking the polymerizing (P-tip) and depolymerizing (D-tip) microtubule from the total number of molecules that reached the microtubule end (mean ± s.e.m.). $n = 8$ independent experiments for full-length CENP-E. Two experiments with truncated CENP-E were analysed by bootstrap analysis with $n = 1{,}000$ samples. Complexes that were observed at the end of the dynamic microtubule for at least 4 s were called tip-tracking. The table shows the number of complexes analysed for each group. (**d**) Kymographs of full-length CENP-E tracking the tip of the growing (upper left panel) and shortening (bottom left panel) microtubules. The right panel shows continuous motion with the end of one dynamic microtubule. (**e**) Histogram of the number of CENP-E dimers in the tip-tracking complexes, showing that a single full-length CENP-E dimer, which contains two GFP fluorophores, can track microtubule tips ($n = 42$ from 3 independent experiments). (**f**) Microtubule velocities and catastrophe frequency in the presence or absence of the tip-tracking full-length CENP-E complexes (containing 1–2 dimers); mean ± s.e.m., $n = 26$ shortening microtubules in each group and $n = 28$ growing microtubules in each group. Tip-tracking by small CENP-E complexes does not significantly affect the rate of growth ($P = 0.22$) and shortening ($P = 0.89$), based on the unpaired t-test. The catastrophe frequency (mean ± s.e.m.) was determined from $n = 6$ independent experiments. The microtubule catastrophe frequency with and without the tracking full-length CENP-E molecules is not significantly different ($P = 0.6$, Mann–Whitney U-test).

the tips of Taxol-stabilized microtubules (Fig. 3b and Supplementary Fig. S2 and Video S3). However, a large fraction of full-length CENP-E molecules did not dissociate from the polymerizing ends and continued to move with microtubule elongation, which was 15 times slower than the motor's walking rate (Fig. 3c,d and Supplementary Fig. S3). This marked slowing is unlikely to result from the different nucleotide composition of the growing tip versus microtubule wall because full-length CENP-E moved only slightly slower on the GMPCPP- versus GDP-containing lattices (Supplementary Fig. S3c). A slower motility on GMPCPP-containing segments was also observed for truncated CENP-E, yet it failed to track processively with the polymerizing tip (Supplementary Fig. S2c).

About 70% of full-length motors that walked into a disassembling microtubule tip also did not dissociate but moved backwards in the direction opposite to the motor-dependent motility, while following the rapidly disassembling microtubule (Fig. 3d and Supplementary Videos S4 and S5). By quantifying the GFP intensity of the tip-tracking complexes we found that many contained only 2 GFP molecules and therefore were dimers of CENP-E (Fig. 3e and Supplementary Fig. S3e–g). The tip-tracking complexes sometimes seemed to diffuse near the tip. This behaviour was more evident at polymerizing tips, presumably because polymerization is 10 times slower than depolymerization (Fig. 3d and Supplementary Video S6). Full-length CENP-E dimers remained associated with growing and shortening tips for 17.9 ± 1.3 and 11.6 ± 1.4 s, respectively, resulting in the travel lengths of 0.3 ± 0.1 and 2.1 ± 0.3 μm (Supplementary Fig. S4a–d and Table S2). Small teams of full-length molecules tracked even better, sometimes remaining at the tip for several rounds of microtubule growth and shortening (Supplementary Video S7). These brighter complexes tended to slow microtubule depolymerization but single tip-tracking dimers did not affect significantly either the rates of growth and shortening, or catastrophe frequency (Fig. 3f). Thus, CENP-E has a capacity to track processively with both assembling and disassembling microtubules at a single-molecule level, a property not shared by previously studied kinesins.

CENP-E can couple microtubule disassembly to bead motion *in vitro*

CENP-E has been observed to localize to the plus ends of spindle microtubules in human cells, consistent with its tip-tracking *in vivo*[15]. Furthermore, previous work implicated CENP-E in assisting motions of isolated mammalian chromosomes at the ends of depolymerizing microtubules *in vitro*[18]. To determine directly whether purified full-length CENP-E can couple microtubule dynamics to cargo

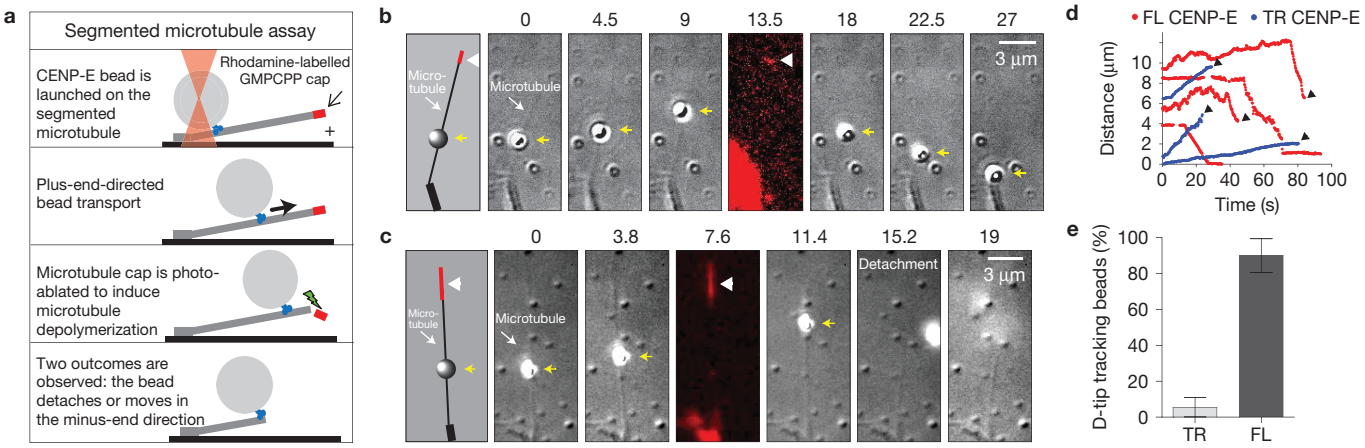

Figure 4 Motion of bead cargo in association with microtubule disassembly. (**a**) Schematics of the segmented microtubule assay *in vitro* using bead cargo. (**b**,**c**) A schematic and still images from a segmented microtubule assay with full-length (**b**) and truncated (**c**) CENP-E-coated beads. The bead (yellow arrowhead) was placed on a capped microtubule grown from a coverslip-attached axoneme, as drawn in the left panel. The fluorescently labelled cap (white arrowhead) was photo-ablated through the rhodamine excitation (red colour). All other images were recorded with differential interference contrast illumination. The numbers above the panels are seconds from the start of the bead's walking. (**d**) Sample motions of the CENP-E-coated beads. Distance is from the minus microtubule end. Arrowheads indicate bead detachment from the microtubule. Full-length CENP-E-coated beads sometimes remained attached even after the microtubule had stopped shortening. (**e**) Tip-tracking frequency of full-length ($n = 10$) and truncated CENP-E-coated beads ($n = 18$). Error bars are s.e.m. estimated by bootstrapping ($n = 1{,}000$ samples).

motion, we used segmented microtubules, an *in vitro* approach we previously developed to study microtubule depolymerization-dependent motions[32] (Fig. 4a). With laser tweezers, CENP-E-coated beads were brought to the walls of microtubules, transiently stabilized by caps made from GMPCPP-containing rhodamine-labelled tubulin. These beads walked towards the capped plus ends, mimicking chromosomal transport during congression. When microtubule depolymerization was triggered by photo-ablating the stabilizing caps, almost all full-length CENP-E-coated beads followed the shortening microtubule ends (Fig. 4b–e), demonstrating the ability of CENP-E to couple bead motions with microtubule disassembly. Such coupling required the non-motor domains of CENP-E as truncated CENP-E-coated beads failed to track (Supplementary Videos S8 and S9).

CENP-E contributes to stable association between depolymerizing microtubule ends and kinetochores

To examine a possible role for CENP-E in linking kinetochores and dynamic microtubule ends, we designed an experiment to trigger chromosome transport by depolymerizing microtubules *in vivo*[33] (Fig. 5a). Monopolar spindles were induced in HeLa cells that expressed the kinetochore marker Mis12–GFP. After chromosomes assumed their positions at the plus tips of astral microtubules, the CENP-E motor was inhibited with GSK-923295, after which microtubule depolymerization was triggered by nocodazole (Fig. 5b). Live imaging of control cells with no CENP-E inhibitor revealed that nocodazole-induced microtubule shortening produced chromosome motion towards the unseparated poles (Fig. 5c,d). Inhibiting CENP-E, however, greatly reduced the ability of chromosomes to move in conjunction with microtubule disassembly (Supplementary Video S10).

To rule out the possibility that the CENP-E inhibitor directly affected microtubule stability, cells were subjected to the same treatments (as in Fig. 5b), but their spindles were visualized with tubulin–EYFP. microtubule depolymerization commenced in <1 min in all cells treated with nocodazole, but adding GSK-923295 alone had no effect (Supplementary Fig. S5). No gross changes in microtubule asters were seen in cells that were fixed and immunostained 25 min after adding GSK-923295, as judged by spindle tubulin intensity (Supplementary Fig. S6). The diameters of microtubule asters were slightly larger in GSK-923295-treated cells, further indicating that this inhibitor did not induce microtubule disassembly (Supplementary Fig. S6c).

Next, cells were pretreated with GSK-923295 for 5 min to deplete CENP-E from the kinetochores, then additionally treated with nocodazole and cold to promote microtubule disassembly. In ~60% of these cells, some chromosomes were left at the periphery with no attached cold-stable microtubule fibres (Fig. 5e,f and Supplementary Fig. S7a). This is a significantly larger fraction than when nocodazole was used with no CENP-E inhibitor, consistent with live imaging results. Furthermore, the GSK-923295 pretreated cells had fewer tubulin-containing microtubule remnants than the cells with CENP-E-depleted kinetochores (Supplementary Fig. S6a,d). Similar results were also seen when CENP-E function was disrupted by RNA-mediated interference (RNAi) in another human cell line and similar experiments were carried out without GSK-923295 (Fig. 5g,h and Supplementary Fig. S7b). We conclude that the presence of the CENP-E motor at the kinetochores promotes their ability to maintain stable connections with disassembling microtubule ends.

Tip-tracking of CENP-E is not caused by its high affinity to microtubule tips, but requires its motor and C-terminal tail

To dissect the molecular mechanisms underlying the processive tip-tracking we tested two specific hypotheses. First, we examined whether tip-tracking could result from the increased affinity of CENP-E to microtubule tips versus walls. With a fluorescence-based microtubule-pelleting assay we measured CENP-E binding to GDP-containing (Taxol-stabilized) microtubules and GMPCPP-containing microtubules that mimick the growing microtubule tips: the apparent dissociation constants were 41 ± 4 nM and 68 ± 23 nM, respectively (Fig. 6a). Binding affinity to the depolymerizing microtubule tips, as

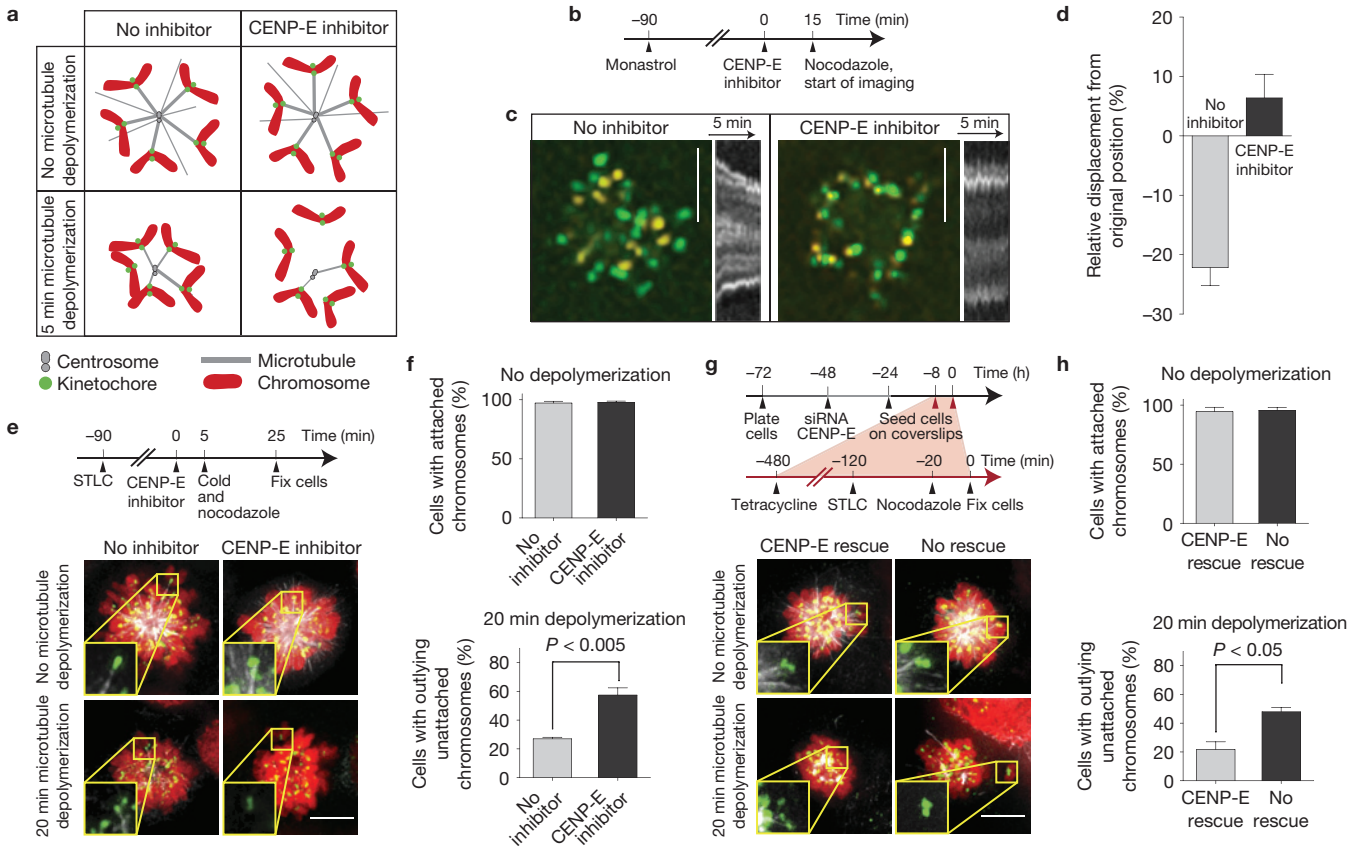

Figure 5 Investigation of the role of CENP-E in depolymerization-driven chromosome motions *in vivo*. (**a**) Schematic diagrams of the microtubule destabilization assay to study chromosome transport by shortening microtubules and summary of the main results. (**b**) Timeline of the microtubule destabilization assay with monopolar spindles in HeLa cells expressing Mis12–GFP (live imaging). (**c**) Two frames of Mis12–GFP kinetochore markers from a time-lapse series for each indicated condition were overlaid to reveal a shift in kinetochore position following the nocodazole-induced microtubule depolymerization (kinetochores in green—before nocodazole treatment; in yellow—5 min after). Greyscale images are the corresponding kymographs (Supplementary Video S10); scans were made across chromosome rosettes. Scale bar, 5 μm. (**d**) Relative change in the position of kinetochores before and 5 min after nocodazole addition (mean ± s.e.m., $n = 10$ cells for each group examined in 4 independent experiments; see equation (1) in Methods). One-way analysis of variance indicates $P < 0.001$, so the means are statistically different. (**e**) Timeline of the microtubule destabilization assay in HeLa cells and representative images (from $n = 3$ independent experiments). Insets show enlarged images of the kinetochores (green) and microtubules (white) at the periphery of the chromosome sphere; note the absence of kinetochore-attached microtubules on the lower right image. The red colour shows DNA (Supplementary Fig. S7a). Scale bar, 5 μm. (**f**) Proportion of HeLa cells with microtubule-attached chromosomes before microtubule depolymerization (top graph) and cells with outlying unattached chromosomes after microtubule depolymerization (bottom graph); chromosomes at the periphery of the chromosome sphere with no attached cold-stable microtubule fibres were scored as outlying unattached chromosomes. Mean ± s.e.m., $n = 3$ independent experiments; P was determined from two-tailed unpaired t test; a total of 87 cells for the inhibitor condition and 89 for the control were examined. (**g**) Timeline of the microtubule destabilization assay with DLD-1 cells and representative images (from $n = 3$ independent experiments); see legend of **e** for details. (**h**) Quantification of kinetochore–microtubule attachment in DLD-1 cells; see legend of **f** for details; mean ± s.e.m., $n = 3$ independent experiments. In total 78 cells were analysed with and 75 with no CENP-E rescue.

measured with tubulin spirals that are similar in structure to the curved tubulin protofilaments[34], was 133 ± 22 nM. Thus, CENP-E shows no significant preference to the tip-mimicking structures, suggesting that its bi-directional tip-tracking is unlikely to result from different affinities.

As truncated CENP-E was unable to track microtubule ends processively, we next investigated whether the C-terminal tail of CENP-E was involved (Fig. 2a). Full-length bound stronger to Taxol-stabilized microtubules than the truncated protein (41 ± 4 nm versus 144 ± 54 nM; Fig. 6a), consistent with the presence of a microtubule-binding site in its tail[26,35]. We expressed and purified a C-terminal CENP-E fragment fused with GFP (Tail, Fig. 6b). This fragment lies distally to the kinetochore-targeting sequence of CENP-E (refs 26,36), so the tails of kinetochore-bound CENP-E molecules may be positioned to interact directly with kinetochore microtubules *in vivo*. Purified Tail molecules bound and diffused rapidly on microtubules but failed to follow the dynamic tips, indicating that tail was not the sole determinant of the bi-directional tip-tracking (Fig. 6c–f). Interestingly, statistical analysis of motions of the Tail at the dynamic microtubule ends has revealed that only 1 out of 10 encounters between the Tail and dynamic microtubule end resulted in Tail's detachment (see Methods), with most Tail molecules bouncing back from the tip and continuing to diffuse along the microtubule wall, as if reflected by the tip (Fig. 6g,h).

A tethered motor mechanism provides a quantitative fit for bi-directional microtubule tip-tracking by CENP-E

On the basis of the above results we then reasoned that even though neither the tail nor the motor domain could track the dynamic microtubule ends on their own, a combination of their molecular

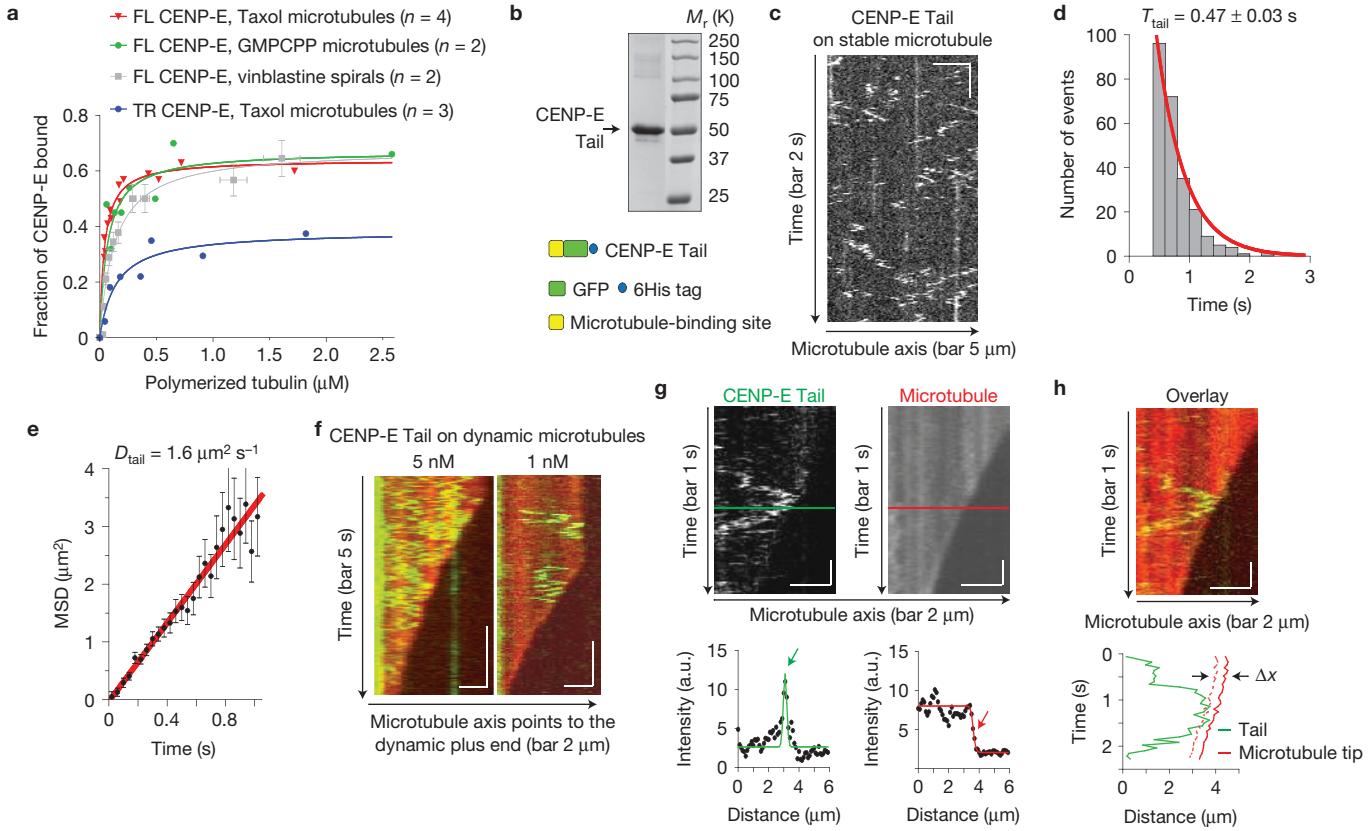

Figure 6 Analysis of possible mechanisms of CENP-E tip-tracking. (**a**) Binding affinity of full-length CENP-E to different tubulin structures. The affinity to the GDP-containing microtubule walls was measured with Taxol-stabilized microtubules; to the growing microtubule ends with GMPCPP-containing microtubules, in which tubulin structure is likely to be similar to that at the polymerizing tips. To mimic curved protofilaments, which are normally seen at the shortening microtubule ends, we used tubulin spirals formed by polymerization in the presence of vinblastine. Points are from individual measurements for a given tubulin concentration; data were collected in *n* independent experiments, as indicated for each curve. Error bars for experiments with vinblastine spirals (mean ± s.e.m.) take into account that on average only 82% of spirals pelleted, whereas other tubulin structures pelleted completely. (**b**) SDS–PAGE of the purified CENP-E Tail protein containing 199 amino acids. (**c**) Kymograph of Tail diffusion. (**d**) Histogram of the residence time of Tail on the microtubule lattice shows that the characteristic residency time for Tail *in vitro* is ~0.5 s ($n = 378$ molecules). (**e**) Mean squared displacement (MSD) for Tail versus time with a linear fit (red). Bars are s.e.m., $n = 433$ molecules. (**f**) Kymographs of Tail (green) on dynamic microtubules (red); there is no processive association with growing or shortening microtubule ends. (**g**,**h**) Quantitative analysis of Tail behaviour at microtubule tips. The upper kymographs in **g** show a Tail molecule diffusing near the shortening end. The intensity profiles along the coloured lines are shown below. Tail and microtubule tip coordinates were determined as described in the Methods. (**h**) Two-colour overlay (top panel) for the same molecule as in **g** but with reconstructed trajectories (bottom graph). The dashed red line marks the distance from the microtubule tip, Δx, that the Tail can travel during 60 ms, the acquisition time for one frame (see equations (2)– (4) in Methods). Tail was scored as reflected from the tip when the Tail was found between the two red lines and then moved away from the tip, as shown in this example.

properties produced a collective tip-tracking behaviour. We tested this hypothesis in a mechanistic and quantitative way with a mathematical model based on the detailed kinetic schemes (Fig. 7a,b). The model describes molecular interactions between the microtubule wall, tip, and the motor and tail domains connected together through a worm-like tether (see Supplementary Note for a detailed description of the model assumptions and Supplementary Table S3 for parameter values). This quantitative model recapitulated the main results of our *in vitro* studies with truncated and full-length CENP-E, including rapid dissociation of the truncated motor from dynamic microtubule ends and the ability of full-length CENP-E to tip-track processively (Fig. 7c–f). It also provided a physical mechanism for the cooperative action of motor and tail domains by demonstrating that full-length CENP-E can track bi-directionally by repeating the cycles of plus-end-directed walking and the tail-mediated diffusion of the microtubule wall-tethered motor (Supplementary Videos S11 and S12). The tail–microtubule wall association, although transient, keeps the tail-tethered motor heads in the vicinity of the microtubule. We estimate that tethered motor heads re-associate with the wall within a millisecond, so the tail serves as a safety leash for the motor heads, which dissociate rapidly and repeatedly from the tip. Remarkably, this behaviour *in silico* does not rely on difference(s) between assembling and disassembling ends, explaining how CENP-E tracks with both types of end.

The proposed tethered motor mechanism of tip-tracking is strongly supported by our experimental observations of diffusive motions of the tip-tracking full-length molecules, as evidenced by the ragged appearance of kymographs (Fig. 8a–c). Several examples of visible excursions at both elongating and shortening microtubule ends are shown in Supplementary Fig. S3d, and the smaller diffusive motions at the tips were common (for example, Supplementary Video S6). We challenged our model by testing experimentally its two key predictions. First, we examined tip-tracking in the presence

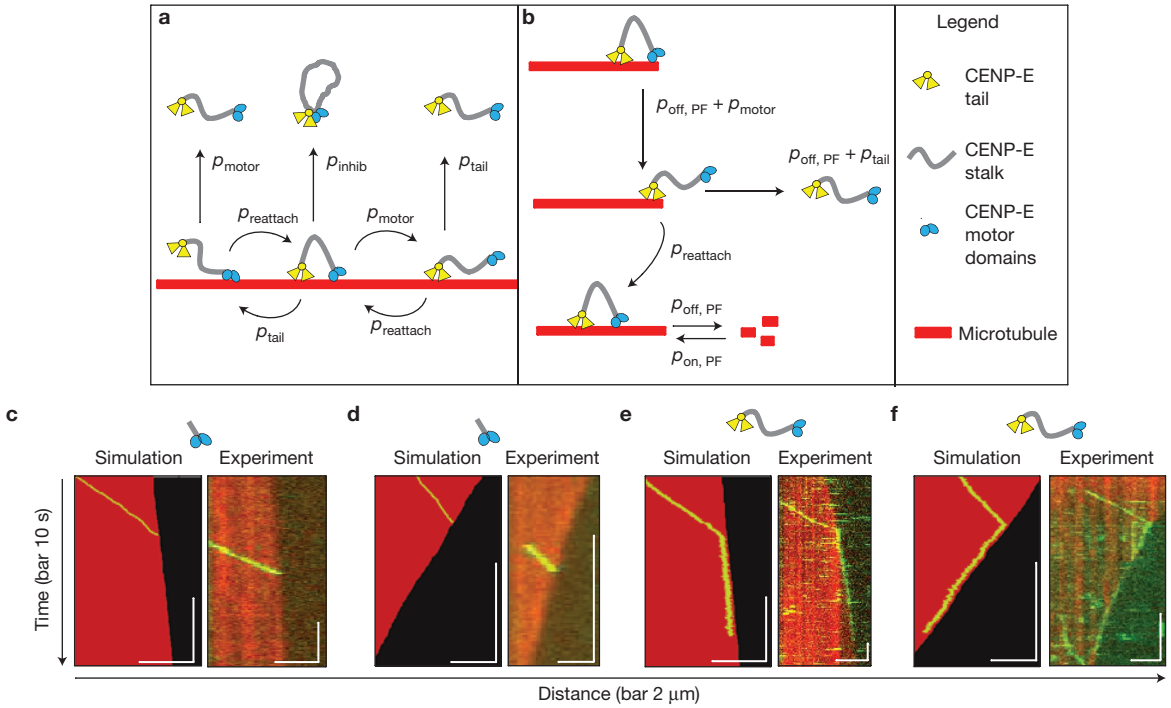

Figure 7 Mathematical model of CENP-E motility and comparison with the results of the *in vitro* study. (**a**,**b**) Kinetic schemes for the *in silico* CENP-E motility on the microtubule lattice (**a**) and the microtubule tip (**b**). The arrows depict the transitions between different kinetic states with the rate constants *p* listed in Supplementary Table S3. (**c**–**f**) Simulated motility kymographs of truncated and full-length CENP-E *in silico* and the representative kymographs for the respective motions *in vitro*. The green lines in the simulated kymographs are the CENP-E coordinates; the red boundary is based on the coordinates of the microtubule ends. Model predictions correspond well with experimental observations; see Supplementary Note for more details.

of the non-hydrolysable ATP analogue AMPPNP, which induces strong microtubule binding. Consistent with the model's prediction, the inhibited full-length CENP-E failed to follow the disassembling microtubule tips (Fig. 8d), demonstrating that the motor's walking is required for processive tip-tracking. Second, we recapitulated the wild-type full-length CENP-E motions by artificially joining the non-tracking truncated CENP-E and Tail proteins. Quantum dots (Qdots) coated with the mixture of these proteins exhibited robust walking and also moved processively with both assembling and disassembling microtubule ends (Fig. 8e). Thus, tail and motor domains cooperate together to provide processive tip association.

DISCUSSION

Here we describe the results of the integrated study of motility of CENP-E kinesin and its physiological implications using *in vivo*, *in vitro* and *in silico* approaches. Experiments in two human cell lines show that kinetochore–microtubule attachments in disassembling monopolar spindles are greatly destabilized when CENP-E function is perturbed with either a specific inhibitor or RNAi depletion. Furthermore, we establish a continuing *in vivo* requirement for CENP-E motor activity at the kinetochores of congressed and bi-oriented chromosomes. Together with our discovery of the ability of CENP-E to associate with the ends of dynamic microtubules *in vitro*, these findings suggest a previously unrecognized function for this essential kinesin in accurate chromosome segregation. We propose that in addition to its established role in transporting polar chromosomes, CENP-E also facilitates the association between kinetochore and dynamic microtubule ends.

In vitro, CENP-E kinesin can convert from a lateral transporter into a microtubule tip-tracker, so a similar activity may contribute to the formation of end-on microtubule attachments for the chromosomes that congress through a kinetochore-fibre-independent pathway[7]. Although a significant fraction of CENP-E protein leaves kinetochores after congression, CENP-E is clearly present at the kinetochores of bi-oriented chromosomes[14,15], and our results *in vivo* establish the physiological role of this CENP-E population in maintaining end-on microtubule attachments. These findings are supported by previous studies in different cell systems including *Drosophila*[37], mouse[11] and human cells[16], and they also provide a molecular mechanism to explain a reduced number of kinetochore microtubules on congressed chromosomes in CENP-E-depleted cells[11,16].

As we have shown that a single dimer of CENP-E can maintain long-lasting association with a dynamic microtubule end *in vitro* without significantly affecting microtubule dynamics, we also propose that a major component of the mechanism underlying CENP-E-mediated stabilization of kinetochore–microtubule attachments is a direct one, provided by its ability to serve as a mobile molecular bond between the kinetochore and dynamic kinetochore–microtubule tip. Future work, however, is required to examine whether the kinetochore-bound CENP-E can also affect dynamics of kinetochore microtubules, because multiple CENP-E molecules may act in concert at kinetochores. Furthermore, in the context of live cells the tip-tracking by CENP-E may promote kinetochore–microtubule attachment not only directly but also in conjunction with additional activities from other associated proteins, such as CLASP1/2 (refs 38,39) or PP1 phosphatase[8].

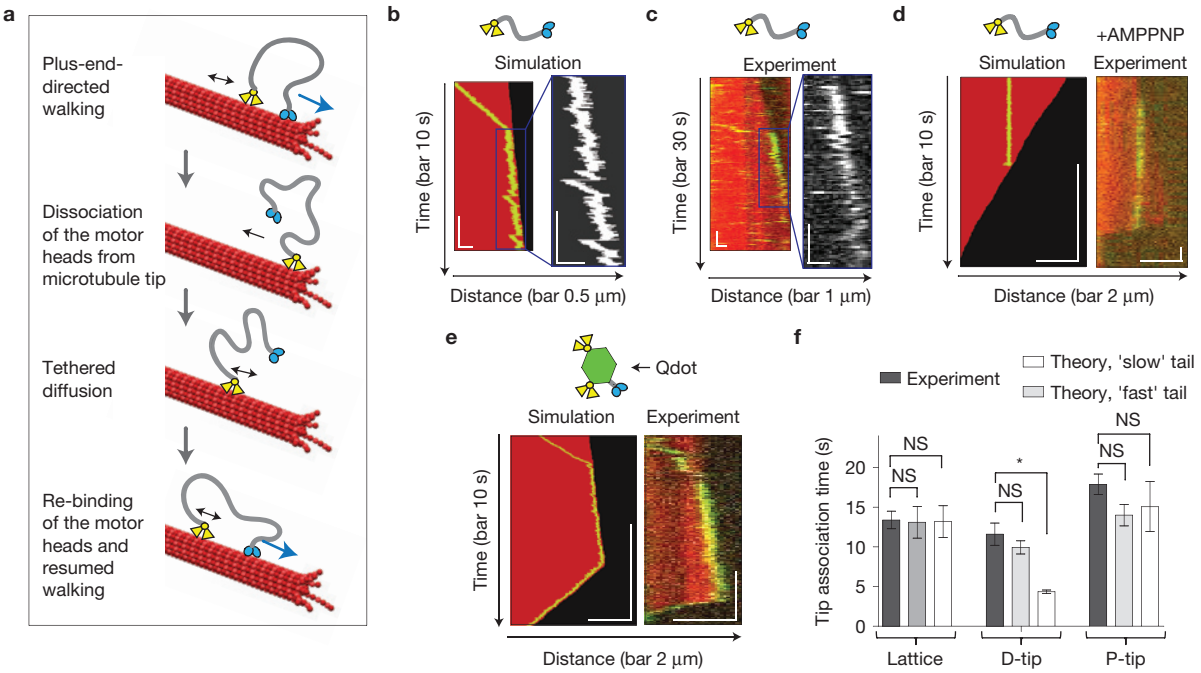

Figure 8 Tethered motor mechanism for processive and bi-directional microtubule tip-tracking and the testing of its predictions. (**a**) Diagram for the tethered motor mechanism of bi-directional tip-tracking. The blue arrow shows unidirectional motor's walking and the black arrows show tails' diffusion and reflection from the tip. (**b**,**c**) Theoretical (**b**) and experimental (**c**) kymographs of the full-length CENP-E tracking of the growing tip. Insets show zooms of the ragged CENP-E tracings, with occasional large, minus-end-directed excursions. Such excursions are explained in the model by the tail-mediated diffusion of the tethered motor. (**d**) Theoretical and experimental kymographs of full-length CENP-E on a shortening microtubule in 2 mM AMPPNP, which blocks motor's walking. The model predicts that the stalled motor should detach when the wave of microtubule depolymerization reaches its attachment site, which is indeed observed *in vitro*. Similar results were seen with GSK-923295, as expected. (**e**) Theoretical and experimental kymographs of Qdot coated with a mixture of truncated CENP-E and Tail proteins. Such dots exhibit the same motile properties as the full-length molecule—they walk on the microtubule wall unidirectionally and convert into bi-directional tip-trackers at the microtubule end. (**f**) Mean lattice and tip-association times for single molecules of full-length CENP-E in the experiment (experimental data are from Supplementary Tables S1 and S2) and as obtained in simulations (theory). The diffusion coefficient of the fast tail *in silico* matches that of the CENP-E Tail protein *in vitro* (Fig. 6e). The slow diffusion coefficient is as reported for the tail of Kif18A (ref. 43). In this range, tail's diffusion has a stronger effect on tracking the depolymerizing, but not polymerizing microtubule ends. Mean ± s.e.m., based on 50 calculations for each motor. $^{*}P < 0.001$; NS, $P > 0.05$ (unpaired t-test).

Our work also provides a detailed molecular mechanism to explain how CENP-E can track microtubule tips processively and bi-directionally. The autonomous tip-tracking that we have uncovered for CENP-E is distinct from that of proteins such as EB1 (end binding 1). Despite being widely referred to as a plus-tip-tracking protein, the individual molecules of EB1 do not associate continuously with growing microtubules and tip-tracking is not processive[40]. Only two proteins, the microtubule polymerase XMAP215 (ref. 23) and Dam1 oligomers[25,41,42], neither with motor activity, have previously been described to track dynamic microtubule tips processively and bi-directionally at a single-molecule level. Members of the kinesin-8 family, the plus-end-directed Kif18A and Kip3, can associate processively with the growing microtubule tip *in vitro*, assisted by their C-terminal tails[43–46]. These motors, however, fail to track disassembling microtubules. The molecular mechanism of their unidirectional plus-end-tracking is not known, so it may include the affinity-based interactions specifically at the assembling tips. Alternatively, kinesin-8 may tip-track with the growing microtubules by the mechanism we propose here for CENP-E. Our computational model provides insight into protein's ability to tip-track uni- versus bi-directionally by emphasizing a complex interrelationship between the rates of protein diffusion and microtubule dynamics[47]. The reported diffusion of the Kif18A tail is 100 times slower than that of the CENP-E tail[43,45]. *In silico*, motors with both tails can travel with the elongating microtubule end quite well because both tails diffuse rapidly relative to the slow rate of microtubule assembly (Fig. 8f). However, the slowly diffusing tail is predicted to dissociate sooner from the shortening microtubule ends because microtubule disassembly is rapid enough to catch up repeatedly with the molecule that diffuses slowly in front of the wave of tubulin depolymerization. Each of these encounters may cause a stochastic loss of the terminal tubulin dimer together with the bound tail molecule, so the slower-diffusing Kif18A tail is not a good tether for the shortening microtubule end. It remains to be seen whether the tethered motor mechanism that we propose is employed by other microtubule-dependent motors, or this specialization is unique to kinetochore-localized kinesin-7. □

METHODS

Methods and any associated references are available in the online version of the paper.

Note: Supplementary Information is available in the online version of the paper

ACKNOWLEDGEMENTS

We thank members of the Grishchuk and Ataullakhanov laboratories for stimulating discussions and technical assistance, A. Korbalev for help with the model videos, M. Porter for a kind gift of axonemes, M. Ostap, M. Lampson and J. R. McIntosh for

critical reading of the manuscript, and E. Ballister and M. Lampson for assistance with live cell imaging. We thank University of California, San Diego, Neuroscience Microscopy Shared Facility (P30 NS047101) and J. R. McIntosh for help with the initial phase of this work (GM 033787). This work has been supported by grants from the NIH to E.L.G. (R01-GM098389) and to D.W.C. (R01-GM29513), and grants to F.I.A from Russian Fund for Basic Research (12-04-00111-a, 13-04-40188-H and RFBR 13-04-40190-H) and Presidium of Russian Academy of Sciences (Mechanisms of the Molecular Systems Integration and Molecular and Cell Biology programmes). B.V. has been supported by a postdoctoral fellowship from the Human Frontiers Science Program. E.L.G. is a Kimmel Scholar; her work is supported in part by the Pennsylvania Muscle Institute. D.W.C. receives salary support from the Ludwig Institute for Cancer Research.

AUTHOR CONTRIBUTIONS

N.G. performed *in vitro* experiments and mathematical modelling; B.V. and A.K. performed *in vivo* experiments; B.V. and Y.K. purified proteins; N.G., B.V., F.I.A., D.W.C. and E.L.G. designed research, analysed data and wrote the paper.

COMPETING FINANCIAL INTERESTS

The authors declare no competing financial interests.

Published online at www.nature.com/doifinder/10.1038/ncb2831
Reprints and permissions information is available online at www.nature.com/reprints

1. Cleveland, D. W., Mao, Y. & Sullivan, K. F. Centromeres and kinetochores: from epigenetics to mitotic checkpoint signaling. *Cell* **112,** 407–421 (2003).
2. Rieder, C. L. & Alexander, S. P. Kinetochores are transported poleward along a single astral microtubule during chromosome attachment to the spindle in newt lung cells. *J. Cell Biol.* **110,** 81–95 (1990).
3. Yang, Z., Tulu, U. S., Wadsworth, P. & Rieder, C. L. Kinetochore dynein is required for chromosome motion and congression independent of the spindle checkpoint. *Curr. Biol.* **17,** 973–980 (2007).
4. Yen, T. J. *et al.* CENP-E, a novel human centromere-associated protein required for progression from metaphase to anaphase. *EMBO J.* **10,** 1245–1254 (1991).
5. Kapoor, T. M. *et al.* Chromosomes can congress to the metaphase plate before biorientation. *Science* **311,** 388–391 (2006).
6. Kim, Y., Heuser, J. E., Waterman, C. M. & Cleveland, D. W. CENP-E combines a slow, processive motor and a flexible coiled coil to produce an essential motile kinetochore tether. *J. Cell Biol.* **181,** 411–419 (2008).
7. Cai, S., O'Connell, C. B., Khodjakov, A. & Walczak, C. E. Chromosome congression in the absence of kinetochore fibres. *Nat. Cell Biol.* **11,** 832–838 (2009).
8. Kim, Y., Holland, A. J., Lan, W. & Cleveland, D. W. Aurora kinases and protein phosphatase 1 mediate chromosome congression through regulation of CENP-E. *Cell* **142,** 444–455 (2010).
9. Schaar, B. T., Chan, G. K., Maddox, P., Salmon, E. D. & Yen, T. J. CENP-E function at kinetochores is essential for chromosome alignment. *J. Cell Biol.* **139,** 1373–1382 (1997).
10. Wood, K. W., Sakowicz, R., Goldstein, L. S. & Cleveland, D. W. CENP-E is a plus end-directed kinetochore motor required for metaphase chromosome alignment. *Cell* **91,** 357–366 (1997).
11. Putkey, F. R. *et al.* Unstable kinetochore-microtubule capture and chromosomal instability following deletion of CENP-E. *Dev. Cell* **3,** 351–365 (2002).
12. Yao, X., Abrieu, A., Zheng, Y., Sullivan, K. F. & Cleveland, D. W. CENP-E forms a link between attachment of spindle microtubules to kinetochores and the mitotic checkpoint. *Nat. Cell Biol.* **2,** 484–491 (2000).
13. Wood, K. W. *et al.* Antitumor activity of an allosteric inhibitor of centromere-associated protein-E. *Proc. Natl Acad. Sci. USA* **107,** 5839–5844 (2010).
14. Brown, K. D., Wood, K. W. & Cleveland, D. W. The kinesin-like protein CENP-E is kinetochore-associated throughout poleward chromosome segregation during anaphase-A. *J. Cell Sci.* **109,** 961–969 (1996).
15. Cooke, C. A., Schaar, B., Yen, T. J. & Earnshaw, W. C. Localization of CENP-E in the fibrous corona and outer plate of mammalian kinetochores from prometaphase through anaphase. *Chromosoma* **106,** 446–455 (1997).
16. McEwen, B. F. *et al.* CENP-E is essential for reliable bioriented spindle attachment, but chromosome alignment can be achieved via redundant mechanisms in mammalian cells. *Mol. Biol. Cell* **12,** 2776–2789 (2001).
17. Weaver, B. A. A. *et al.* Centromere-associated protein-E is essential for the mammalian mitotic checkpoint to prevent aneuploidy due to single chromosome loss. *J. Cell Biol.* **162,** 551–563 (2003).
18. Lombillo, V. A., Nislow, C., Yen, T. J., Gelfand, V. I. & McIntosh, J. R. Antibodies to the kinesin motor domain and CENP-E inhibit microtubule depolymerization-dependent motion of chromosomes *in vitro*. *J. Cell Biol.* **128,** 107–115 (1995).
19. Hirokawa, N., Noda, Y., Tanaka, Y. & Niwa, S. Kinesin superfamily motor proteins and intracellular transport. *Nat. Rev. Mol. Cell Biol.* **10,** 682–696 (2009).
20. McIntosh, J. R., Grishchuk, E. L. & West, R. R. Chromosome-microtubule interactions during mitosis. *Annu. Rev. Cell Dev. Biol.* **18,** 193–219 (2002).
21. Walczak, C. E., Cai, S. & Khodjakov, A. Mechanisms of chromosome behaviour during mitosis. *Nat. Rev. Mol. Cell Biol.* **11,** 91–102 (2010).
22. Rieder, C. L. & Salmon, E. The vertebrate cell kinetochore and its roles during mitosis. *Trends Cell Biol.* **8,** 310–318 (1998).
23. Brouhard, G. J. *et al.* XMAP215 is a processive microtubule polymerase. *Cell* **132,** 79–88 (2008).
24. Westermann, S. *et al.* The Dam1 kinetochore ring complex moves processively on depolymerizing microtubule ends. *Nature* **440,** 565–569 (2006).
25. Lampert, F., Hornung, P. & Westermann, S. The Dam1 complex confers microtubule plus end-tracking activity to the Ndc80 kinetochore complex. *J. Cell Biol.* **189,** 641–649 (2010).
26. Espeut, J. *et al.* Phosphorylation relieves autoinhibition of the kinetochore motor Cenp-E. *Mol. Cell* **29,** 637–643 (2008).
27. Lu, H., Ali, M. Y., Bookwalter, C. S., Warshaw, D. M. & Trybus, K. M. Diffusive movement of processive kinesin-1 on microtubules. *Traffic* **10,** 1429–1438 (2009).
28. Yardimci, H., van Duffelen, M., Mao, Y., Rosenfeld, S. S. & Selvin, P. R. The mitotic kinesin CENP-E is a processive transport motor. *Proc. Natl Acad. Sci. USA* **105,** 6016–6021 (2008).
29. Coy, D. L., Hancock, W. O., Wagenbach, M. & Howard, J. Kinesin's tail domain is an inhibitory regulator of the motor domain. *Nat. Cell Biol.* **1,** 288–292 (1999).
30. Shastry, S. & Hancock, W. O. Interhead tension determines processivity across diverse N-terminal kinesins. *Proc. Natl Acad. Sci. USA* **108,** 16253–16258 (2011).
31. Sardar, H. S., Luczak, V. G., Lopez, M. M., Lister, B. C. & Gilbert, S. P. Mitotic kinesin CENP-E promotes microtubule plus-end elongation. *Curr. Biol.* **20,** 1648–1653 (2010).
32. Grishchuk, E. L., Molodtsov, M. I., Ataullakhanov, F. I. & McIntosh, J. R. Force production by disassembling microtubules. *Nature* **438,** 384–388 (2005).
33. Inoue, S. The effect of colchicine on the microscopic and submicroscopic structure of the mitotic spindle. *Exp. Cell Res.* **2 (suppl.),** 305–318 (1952).
34. Marantz, R. & Shelanski, M. L. Structure of microtubular crystals induced by vinblastine *in vitro*. *J. Cell Biol.* **44,** 234–238 (1970).
35. Liao, H., Li, G. & Yen, T. J. Mitotic regulation of microtubule cross-linking activity of CENP-E kinetochore protein. *Science* **265,** 394–398 (1994).
36. Chan, G. K., Schaar, B. T. & Yen, T. J. Characterization of the kinetochore binding domain of CENP-E reveals interactions with the kinetochore proteins CENP-F and hBUBR1. *J. Cell Biol.* **143,** 49–63 (1998).
37. Yucel, J. K. *et al.* CENP-meta, an essential kinetochore kinesin required for the maintenance of metaphase chromosome alignment in *Drosophila*. *J. Cell Biol.* **150,** 1–11 (2000).
38. Maffini, S. *et al.* Motor-independent targeting of CLASPs to kinetochores by CENP-E promotes microtubule turnover and poleward flux. *Curr. Biol.* **19,** 1566–1572 (2009).
39. Maia, A. R. R. *et al.* Cdk1 and Plk1 mediate a CLASP2 phospho-switch that stabilizes kinetochore-microtubule attachments. *J. Cell Biol.* **199,** 285–301 (2012).
40. Dixit, R. *et al.* Microtubule plus-end tracking by CLIP-170 requires EB1. *Proc. Natl Acad. Sci. USA* **106,** 492–497 (2009).
41. Gestaut, D. R. *et al.* Phosphoregulation and depolymerization-driven movement of the Dam1 complex do not require ring formation. *Nat. Cell Biol.* **10,** 407–414 (2008).
42. Grishchuk, E. L. *et al.* Different assemblies of the DAM1 complex follow shortening microtubules by distinct mechanisms. *Proc. Natl Acad. Sci. USA* **105,** 6918–6923 (2008).
43. Stumpff, J. *et al.* A tethering mechanism controls the processivity and kinetochore-microtubule plus-end enrichment of the kinesin-8 Kif18A. *Mol. Cell* **43,** 764–775 (2011).
44. Su, X. *et al.* Mechanisms underlying the dual-mode regulation of microtubule dynamics by Kip3/kinesin-8. *Mol. Cell* **43,** 751–763 (2011).
45. Mayr, M. I., Storch, M., Howard, J. & Mayer, T. U. A non-motor microtubule binding site is essential for the high processivity and mitotic function of kinesin-8 Kif18A. *PLoS ONE* **6,** e27471 (2011).
46. Weaver, L. N. *et al.* Kif18A uses a microtubule binding site in the tail for plus-end localization and spindle length regulation. *Curr. Biol.* **21,** 1500–1506 (2011).
47. Grishchuk, E. L., McIntosh, J. R., Molodtsov, M. I. & Ataullakhanov, F. I. *Comprehensive Biophysics* Vol. 4, 93–117 (Elsevier B.V, 2012).

METHODS

Statistical analysis. Graphics and statistical analyses for all figures were carried out using GraphPad Prism software. All results represent the mean ± s.e.m., unless stated otherwise. Bootstrap estimation of standard errors was carried out with Matlab. Box-and-whiskers plots show the minimum to maximum range of the data. The significance of differences between the means or the population distributions was determined using the Mann–Whitney two-tailed test (Fig. 3f columns for microtubule catastrophe frequency), two-tailed unpaired Student t-test (Figs 1c and 3f for microtubule velocities; Figs 5f,h and 8f and Supplementary Fig. S3c and Supplementary Fig. S6b–d) and one-way analysis of variance test (Fig. 5d). For all tests, differences were considered statistically significant if P values were less than 0.05 (as indicated with *).

Cell culture and immunofluorescence. Cells were maintained at 37 °C with 5% CO_2 in Dulbecco's modified Eagle's medium containing 10% tetracycline-free fetal bovine serum (Clontech), 100 U ml^{-1} penicillin, 100 U ml^{-1} streptomycin and 2 mM L-glutamine. The CENP-E rescue experiment was performed using the full-length human CENP-E open reading frame cloned in a pcDNA5/FRT/TO vector (Invitrogen), generated as described previously[8]. Doxycycline was used at 1 mg ml^{-1} to induce GFP–CENP-E expression in DLD-1 cells. For siRNA treatment Flp-In truncatedex-DLD-1 H2B–RFP cells and HeLa H2B–RFP, tubulin–EYFP were used as described previously[8]. Cells were processed for immunofluorescence 48 h after siRNA treatment by fixing in 4% formaldehyde in microtubuleSB (100 mM PIPES at pH 6.8, 0.1% Triton X-100, 0.1 mM $CaCl_2$ and 1 mM $MgCl_2$) and blocking overnight at 4 °C in 2.5% FBS, 0.2 M glycine and 0.1% Triton X-100 in PBS, followed by 1 h antibody incubation. CENP-E antibody HpX-1 (ref. 14), anti-tubulin antibody DM1A (Sigma, T9026) and anti CENP-A antibody (Abcam, Ab 13939) were used at 1:1,000; anti-centromere antibody ACA (Antibodies Incorporated, 15-234-0001) at 1:500. Cells were mounted in ProLong Gold (Invitrogen). Monopolar spindles were formed with 5 μM S-trityl-L-cysteine (STLC) for 2 h and 20 μM MG132 to prevent mitotic exit; GSK-923295 was used at 200 nM. To induce microtubule disassembly in cells with monopolar spindles, cells were treated for 20 min with a combination of 3.3 μM nocodazole and cold by incubating on a slurry of ice and water. Cells were fixed and immunostained; images were collected at 0.2 μm z-sections with a ×100 1.35 NA oil objective using a DeltaVision Core system (Applied Precision) with a Coolsnap camera (Roper). Images were deconvolved with SoftWoRx (Applied Precision) and maximum-intensity two-dimensional projections were assembled using FIJI (ImageJ, NIH). The microtubule signal was quantified by measuring the total pixel intensity of the entire microtubule rosettes using FIJI, and local background was subtracted; the same cells were used to measure the diameter of microtubule asters. The number of the repeats for each experiment is described in the corresponding figure legends.

Live-cell imaging. HeLa cells expressing tubulin–EYFP and histone H2B–mRFP (for bipolar spindles), or cells with Mis12–GFP (for monopolar spindles; cells kindly provided by E. Ballister and M. Lampson, University of Pennsylvania, USA) were used. To study bipolar spindles, cells were seeded 24 h before the experiment in Nunc Labtek II chambered coverglasses (Thermo Scientific). After adding 100 nM Velcade for 1 h, cells were washed, transferred to the CO_2-independent medium (Gibco) containing 200 nM GSK-923295 or an equal volume of DMSO and imaged at 37 °C for 1 h at 2 min intervals and 1 μm z-sections (10 s) with a ×60 1.42 PlanApo N oil objective using a DeltaVision Core system. Image analysis and processing was performed as above. Monopolar spindles were induced with 100 μM monastrol in L15 medium with 10% FBS and antibiotics for 90 min and observed with a confocal microscope (Leica) at 37 °C. While on a microscope stage, cells were treated with 200 nM GSK-923295 or an equal volume of DMSO (control) for 15 min, and then 10 μM nocodazole was added. Images of Mis12–GFP marker were acquired in 3 different Z-planes with a 0.5 μm step every 10 s for 5 min with a Hamamatsu camera controlled by MetaMorph. Photos (Fig. 5c) and Supplementary Video S10 are maximum-intensity projections. Kymographs were created with MetaMorph using time-lapse sequences as in Supplementary Video S10. This program was also used to collect X_i and Y_i kinetochore positions for each cell and their centre of mass was calculated with Microsoft Excel as $X_{\text{centre}} = \sum_i^N X_i/N$, $Y_{\text{centre}} = \sum_i^N Y_i/N$, where N is the total number of observed kinetochores for each cell (8–30 with an average of 16). The corresponding variance for each cell and for different times after the addition of nocodazole was calculated as

$$\sigma = \sqrt{\sum_i^N ((X_i - X_{\text{center}})^2 + (Y_i - Y_{\text{center}})^2)/N} \quad (1)$$

Relative displacement of the kinetochore positions (plotted in Fig. 5d) was calculated as $(\sigma_5 - \sigma_0)/\sigma_0 \times 100\%$, where the subscript is the time in minutes after the addition of nocodazole. Negative net displacement corresponds to poleward chromosome motions; changes in the kinetochore positions in GSK-923295 are not statistically significantly different from 0.

Protein purification. Tubulin was purified from cow brains by thermal cycling and chromatography, and then labelled with rhodamine, biotin or Hilyte647 (ref. 48). *Xenopus laevis* truncated CENP-E labelled with GFP was expressed and purified from *Escherichia coli* as in ref. 6. *Xenopus laevis* full-length CENP-E was expressed and purified from High Five cells (Invitrogen)[49]. For single-molecule assays, full-length CENP-E was dialysed against BRB80 (80 mM PIPES, 1 mM $MgCl_2$ and 1 mM EGTA, at pH 6.9) supplemented with 1 mM dithiothreitol (DTT) and diluted with 4 volumes of 1.25× motility buffer. About half of our data were obtained with full-length CENP-E purified as in ref. 8. The conventional transport motility and microtubule tip-tracking of proteins purified with or without the chromatographic step were similar, so these data were combined. The CENP-E Tail construct was prepared by fusing the last 199 residues of CENP-E with C-terminal EGFP and 6His tags in a pET21a(+) vector (Novagen). Expression was induced at 13 °C for 14 h with 20 μM IPTG in Rosetta cells (DE3); bacterial pellets were lysed with lysozyme (1 mg ml^{-1}) on ice for 30 min and sonication in 25 mM K-PIPES, at pH 6.8, 300 mM KCl, 20 mM imidazole, 5 mM $MgCl_2$, 0.5 mM EGTA, 10 mM β-mercaptoethanol, 1 mM phenylmethylsulphonyl fluoride and protease inhibitors from a cocktail tablet (Roche). After centrifugation at 32,572g (Sorvall SA-600 rotor) for 30 min, the supernatant was incubated with Ni–nitrilotriacetic acid (QIAGEN) for 1 h at 4 °C. The protein was further purified by HiTrap SP HP (GE Healthcare) using a 100 mM–1 M KCl gradient in 25 mM PIPES, at pH 6.8, 5 mM $MgCl_2$ and 1 mM DTT. The peak fraction from the sulphopropyl column was then loaded onto Superose 12 10/300 GL (GE Healthcare) and run using 25 mM K-PIPES, at pH 6.8, 100 mM KCl, 5 mM $MgCl_2$, 0.5 mM EGTA, 1 mM DTT and 20% sucrose. The peak fractions were collected (Fig. 6b).

Fluorescence-based microtubule-pelleting assay. Rhodamine-labelled (1:20) tubulin was used to grow the Taxol-stabilized microtubules as described previously[48] but DMSO was substituted with 25% glycerol, and the GMPCPP microtubules were polymerized with 6.2 mg ml^{-1} tubulin in BRB80 buffer with 1 mM GMPCPP for 15 min at 37 °C and isolated by centrifugation. Tubulin spirals were generated as described previously[50] by incubating 1 mg ml^{-1} of rhodamine-labelled tubulin in MES buffer (100 mM MES, at pH 6.4, 1 mM $MgCl_2$, 1 mM EGTA, 0.1 mM EDTA and 1 mM DTT) with 10 μM vinblastine for 30 min at 37 °C. The spirals were centrifuged in an airfuge (Airfuge A-100/18 rotor, Beckman Coulter) at 126,000g for 30 min, resuspended in BRB80 buffer with 10 μM vinblastine and used immediately. CENP-E proteins were dialysed into BRB80 1 mM DTT for 1 h at 4 °C, then diluted to 6 nM, incubated for 15 min with tubulin structures in binding buffer (BRB80, 2 mM ADP, 4 mg ml^{-1} BSA, 2 mM DTT and 10 μM Taxol or vinblastine) and spun at 81,000g for 3 min for microtubules or at 126,000g for 30 min for spirals. Supernatants were collected and the average pixel brightness of images was compared with the brightness of standard GFP-labelled protein with concentration determined by GFP absorbance. The fraction of CENP-E bound to tubulin structures was calculated from the total amount of CENP-E added and the amount of unbound protein determined on the basis of the supernatant's fluorescent brightness. Concentration of tubulin structures was determined by depolymerizing them on ice overnight in the presence of 20 mM $CaCl_2$ and measuring the rhodamine intensity of these solutions. The binding affinity K_d was estimated by fitting data with $Y = B_{\max} \times x/(K_d + x)$, where $B_{\max}$ is the intensity at saturation and K_d values are reported with 95% confidence.

Single-molecule TIRF motility assays. We used a Nikon Eclipse Ti-E inverted microscope equipped with a 1.49 NA TIRF ×100 oil objective, Perfect Focus system and TIRF Quad cube with emission wheels run with NIS-Elements Software. The temperature of the objective was kept at 32 °C with a heater (Bioptechs). The epi-fluorescence was excited by rapidly switching between a 488 nm diode 100 mW laser and a CUBE 640 nm diode 70 mW laser (Coherent) using an acousto-optical tunable filter. CENP-E motility was imaged at 100 ms per frame for each channel, acquired with an Andor electron-multiplying CCD (charge-coupled device). CENP-E Tail diffusion was recorded continuously with 20 ms exposure time; dots were tracked as in Fig. 6g and the diffusion coefficient was determined from the slope of the mean squared displacement versus time (Fig. 6e). All single-molecule observations were carried out using at least 2 experimental microscopy chambers.

For assays with stable microtubules, chambers were prepared with a glass slide, double-sided sticky tape and silanized 22 mm × 22 mm coverslips[51]. Taxol-stabilized rhodamine-labelled microtubules were attached through anti-tubulin antibodies (Serotec), the surface was blocked with Pluronic-F127 and GFP-labelled proteins were imaged in the motility buffer (BRB80 with 4 mg ml^{-1} BSA, 2 mM DTT, 2 mM Mg–ATP, 50 μg ml^{-1} glucose, 68 μg ml^{-1} catalase, 0.1 mg ml^{-1} glucose oxidase and 0.5% β-mercaptoethanol) supplemented with 7.5–10 μM Taxol.

DOI: 10.1038/ncb2831

For experiments with dynamic microtubules, microtubule seeds were made from a mixture of unlabelled, rhodamine-labelled and biotin-labelled tubulins and 1 mM GMPCPP (Jena Bioscience). Custom-made perfusion chambers[32] were functionalized with 5 mg ml^{-1} biotin–BSA, then 1 mg ml^{-1} streptavidin, followed by 1% pluronic F127 and 1 mg ml^{-1} casein (10 min incubations with intermittent washing). The dynamic microtubule extensions were formed from tubulin labelled with Hilyte647 and imaged as above at 100 ms per frame, but several videos were recorded using dimly labelled rhodamine–tubulin. In this case, excitation for both tubulin and GFP–CENP-E was carried out with a 488 nm laser at 1.3 s per 1 set of images, and the microtubule image was then separated spectrally using a rhodamine emission filter (with this method, the brightly labelled seeds were visible in the GFP channel). To provide a consistent definition of the tip-tracking event observed with different imaging techniques, only those complexes that remained at the microtubule tip for at least 4 s were called tip-tracking. This time was sufficient to acquire 3 sets of 2-colour images with rhodamine-labelled tubulin (one laser illumination) and 20 sets with Hilyte647-labelled tubulin (two lasers illumination). Dynamic microtubules were grown with 5 μM tubulin in motility buffer supplemented with 1 mM Mg–GTP, 1 mg ml^{-1} casein and 0.15–0.3% methyl cellulose. The final CENP-E concentration was 2–10 nM. In some experiments, microtubule shortening was induced by removing soluble tubulin. The rate of microtubule shortening and elongation with and without tip-tracking complexes was estimated on the basis of the corresponding kymographs; these data were collected in 4 independent experiments. The catastrophe frequency was determined from 6 independent experiments, in which a total of 450 microtubule catastrophes were recorded during 50.6 h for microtubules with no CENP-E. Five microtubule catastrophes were observed for 41 polymerizing microtubule tips that had the tip-tracking CENP-E complexes during a total observation time of 23.9 min (Fig. 3f).

For Qdots experiments we coated streptavidin-conjugated Qdots585 (Invitrogen) with biotinylated anti-GFP antibody (ABCAM) in a 1:3 molar ratio on ice for 1 h, truncated CENP-E and Tail proteins were then added for 1 h. The molar ratio of Qdots/truncated CENP-E/CENP-E Tail was 1:3:30. Immediately before the experiment the mix was diluted 100-fold in the motility buffer and assayed as described above. Fluorescence of Qdots and Hilyte647 tubulin was excited using 488 nm and 640 nm lasers, respectively, and emission was collected with a 580 nm long-pass filter.

Size of the tip-tracking CENP-E complexes. Kymographs of the walking CENP-E–GFP molecules were analysed by drawing the line scans along these trajectories and building the corresponding intensity distribution (Supplementary Fig. S3e–g). The photobleaching step was identified from this multi-peak distribution as in ref. 42, and used as a unit of GFP intensity for quantification of the size of tip-tracking CENP-E complexes in the kymographs.

Quantitative analysis of the interactions between CENP-E Tail and the dynamic microtubule tips. To examine Tail's behaviour at the microtubule end, we used kymographs exhibiting a landing of a single Tail molecule on the microtubule lattice, its diffusion near the microtubule tip and eventual detachment from the microtubule (such as Fig. 6f,h). Tail's coordinates X during these motions were determined by the Gaussian fits of the Tail–GFP intensity line scans using Matlab (Fig. 6g). microtubule tip coordinates were determined by fitting the intensity line scans with the sigmoid function as in equation (2):

$$I(x) = I_{BG} + (I_{microtubule} - I_{BG})\frac{1}{1+10^{x-C}} \quad (2)$$

where I_{BG} and $I_{microtubule}$ are the intensity of the microtubule-free background and microtubule, respectively (Fig. 6g); x is the coordinate along the microtubule axis and the parameter C defines the position of the microtubule tip.

Using this approach we identified $N_{total} = 33$ kymographs, in which Tail's coordinate X was found within the distance Δx from the microtubule tip C at least once:

$$C > X \geq C - \Delta x \quad (3)$$

where

$$\Delta x = \sqrt{2D_{tail}\tau} \quad (4)$$

is the average distance that the Tail with coefficient D_{tail} can travel during time τ, the interval between two consecutive images. This distance reflects the limited accuracy with which one can determine that the Tail has contacted the tip at this frame rate. Owing to the random nature of diffusion, the Tail molecule that is found within the Δx distance from the microtubule end will encounter the terminal microtubule dimer during time τ with the same probability as the probability that it reverses its motion and does not reach the microtubule end. This simple consideration suggests that only about half of the observed diffusion events should have resulted in the Tail reaching the microtubule terminus, suggesting that $N_{encounters} = 16.5$. This intuitive estimate was verified by calculating explicitly the number of Tail–tip encounters during n frames of continuous observation with exposure time τ:

$$N_{encounters} = \sum_{i=1}^{n} P(x \geq X_i + \Delta x_i) = n - \sum_{i=1}^{n} \int_{-\infty}^{X_i+\Delta x_i} \sqrt{\frac{1}{4\pi D_{tail}\tau}}\, e^{-(x-X_i)^2/4D_{tail}\tau} dx \quad (5)$$

where subscript i refers to the experimental values corresponding to the ith frame, and $P(x \geq X_i + \Delta x_i)$ is the probability that the Tail diffuses farther than Δx_i from its initial position X_i during time τ. Equation (5) was applied for the selected 33 diffusion tracings, where $N = 247$, $\tau = 0.06$ s and $D_{tail} = 1.6\,\mu m^2\,s^{-1}$, leading to $N_{encounters} = 16.2 \pm 2.8$, which confirms the intuitive estimate.

The probability F of the Tail detachments from the microtubule tip was then calculated as follows:

$$F = N_{detachments}/N_{encounters} \quad (6)$$

where $N_{detachments}$ is the number of the Tail detachments from the tip and $N_{encounters}$ is the number of Tail–tip encounters. Furthermore,

$$N_{detachments} = N_{total} - T_{total}/T_{tail} \quad (7)$$

where T_{total} is the total time of observation and T_{tail} is the lifetime of Tail's diffusion on the microtubule lattice. Using the experimentally measured values $T_{tail} = 0.47 \pm 0.03$ s and $T_{total} = 14.8$ s (total of 247 acquisition frames with 0.06 s exposure), equation (7) yields $N_{detachments} = 1.5 \pm 2.0$. Using equation (6) we obtain $F = (9.3 \pm 6.3)\%$. Thus, the experimentally observed number of times that Tail detached from the tip is at least 10 times lower than what is expected if the Tail detached every time it reached the end of the polymer track.

Work with CENP-E-coated beads. Our laser trap instrument was described previously[52]. COOH-activated glass beads (0.5 μm, Bangs Laboratories) were coated with streptavidin[42], functionalized with biotinylated anti-GFP antibodies (Rockland) or biotinylated anti-6His tag antibody (Abcam), incubated with CENP-E at 4 °C for 4 h, washed and stored on ice. Motility was examined for 2 days without a visible loss of activity using bead motility buffer (BRB80 with 1 mM $MgCl_2$, 4 mg ml^{-1} BSA, 2 mM DTT, 2 mM Mg–ATP, 50 μg ml^{-1} glucose, 68 μg ml^{-1} catalase, 0.1 mg ml^{-1} glucose oxidase, 0.5% β-mercaptoethanol and 7.5 μM Taxol). Beads were captured with a strong trap (stiffness 0.02 pN nm^{-1}), brought close to Taxol-stabilized, coverslip-attached microtubules. The trap stiffness was then reduced to 0.0025 pN nm^{-1}, and the piezo-stage was moved up and down ≥10 times with 0.5 μm steps to promote bead–microtubule binding. The trap was turned off as soon as the bead's directional motility was detected. Images were recorded in differential interference contrast with 100 ms exposure. A bead was considered motile if it walked ≥0.6 μm from the trap's centre. The assay with segmented microtubules was carried out as described previously[32], and the above procedure was followed to promote the bead's binding to the GDP-segment of the microtubule wall. After the plus-end-directed motility of the CENP-E-coated bead was observed, the microtubule cap was photo-ablated to induce microtubule depolymerization by illumination through the Texas red filter cube. The resulting images were analysed in MetaMorph to construct distance-versus-time bead curves (Fig. 4d).

Comparison of full-length CENP-E activity in the beads and TIRF assays. We used the average integral brightness B of a CENP-E–GFP-coated bead as a measure proportional to the number of motors on a bead. Assuming that the probability for an active bead-associated motor to bind an microtubule within a certain time follows a Poisson distribution[53], the chance that a bead with brightness B has at least one active motor is described with the following equation:

$$P(N \geq 1) = 1 - e^{-\sigma B} \quad (8)$$

where σ depends on the activity of CENP-E preparation and acquisition settings. Fitting of data in Supplementary Fig. S1g with equation (8) shows that full-length CENP-E-coated beads were threefold less active than the truncated CENP-E beads ($\sigma_{truncated} = (3.0 \pm 0.14) \times 10^{-6}$ a.u.; $\sigma_{full-length} = (0.89 \pm 0.26) \times 10^{-6}$ a.u.). To evaluate the relative activity of CENP-E proteins in the single-molecule TIRF assay, we measured the number of unidirectional walks >0.6 μm per unit microtubule length per time interval at 2 nM motor concentration: full-length CENP-E recordings produced 26 such events on 157 microtubules (total length 1.5 mm), whereas the truncated CENP-E motor had 486 walks on 166 microtubules (total length 2.0 mm). Each microtubule was observed for 90 s. Thus, the activity of cargo-free full-length CENP-E is 7% from the activity of the cargo-free truncated

CENP-E molecules. This is a significantly larger difference than we measured for these proteins in the bead assays (30%; Supplementary Fig. S1h), suggesting that binding to bead cargo activates full-length CENP-E.

Computer modelling. A detailed description of the mathematical model of CENP-E motility is provided in the Supplementary Note. All parameters and their values are provided in Supplementary Table S3. Matlab code is available on request.

48. Hyman, A. *et al*. Preparation of modified tubulins. *Meth. Enzymol.* **196,** 478–485 (1991).
49. Abrieu, A., Kahana, J. A., Wood, K. W. & Cleveland, D. W. CENP-E as an essential component of the mitotic checkpoint *in vitro*. *Cell* **102,** 817–826 (2000).
50. Ludueña, R. F., Fellous, A., Francon, J., Nunez, J. & McManus, L. Effect of tau on the vinblastine-induced aggregation of tubulin. *J. Cell Biol.* **89,** 680–683 (1981).
51. Helenius, J., Brouhard, G., Kalaidzidis, Y., Diez, S. & Howard, J. The depolymerizing kinesin MCAK uses lattice diffusion to rapidly target microtubule ends. *Nature* **441,** 115–119 (2006).
52. Grishchuk, E. L. *et al*. The Dam1 ring binds microtubules strongly enough to be a processive as well as energy-efficient coupler for chromosome motion. *Proc. Natl Acad. Sci. USA* **105,** 15423–15428 (2008).
53. Svoboda, K. & Block, S. M. Force and velocity measured for single kinesin molecules. *Cell* **77,** 773–784 (1994).

nature cell biology

DOI: 10.1038/ncb2831

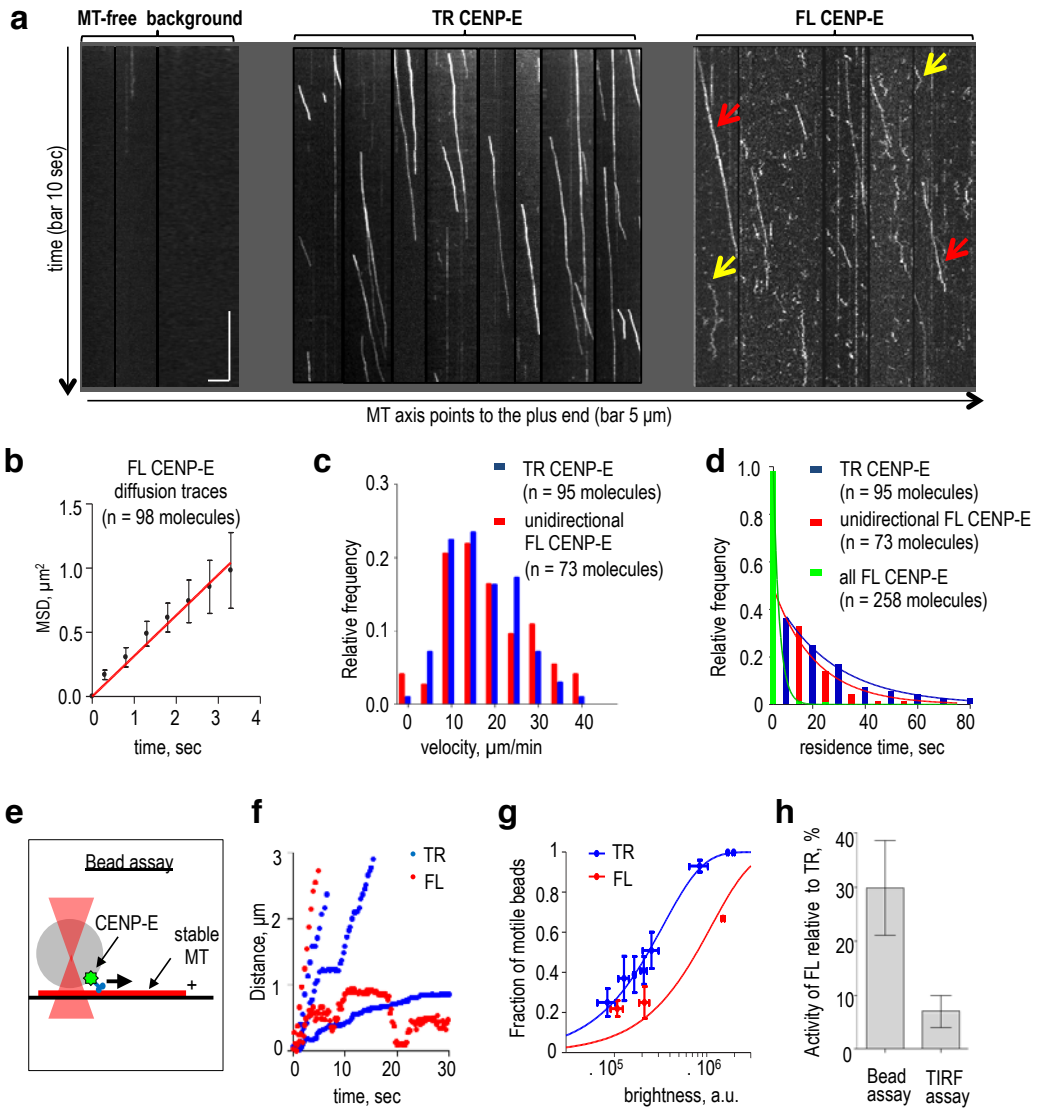

Figure S1 Motility of single CENP-E molecules on stable MTs in TIRF and bead assays. (**a**) Representative kymographs of GFP-labeled CENP-E molecules (1-4 nM) on Taxol-stabilized MTs. The majority of TR CENP-E molecules that land on MTs show unidirectional and processive motility. FL CENP-E molecules associate with MTs on average for a much shorter time (compare with kymographs from scans in the same chambers but away from MTs on the left panels). The unidirectionally walking molecules (red arrows), as well as the diffusing ones (yellow), are also readily observed. (**b**) Mean squared displacement (MSD) of diffusing FL CENP-E molecules as a function of time, bars are SEM. Red line is a linear fit, which corresponds to the diffusion coefficient 0.16±0.01 μm^2/sec (Mean ± SEM) **(c, d)** Histograms of the velocity and residence time of different CENP-E proteins, as determined in TIRF assay. "All FL CENP-E" correspond to data from all visible events, including short-lived interactions, diffusion and unidirectional walking. (**e**) Schematics of the bead motility assay. Red cones symbolize a focused trapping laser beam. (**f**) Example distance vs. time curves for CENP-E-coated beads moving on Taxol-stabilized MTs; some beads coated with FL CENP-E showed diffusive motions, similar to behavior of bead-free FL CENP-E molecules, see panel a. (**g**) Fraction of motile beads as a function of their binned integral GFP brightness. Data are Mean ± SEM, based on 20 independent experiments with TR CENP-E (n = 360 beads), and 4 independent experiments with FL CENP-E (n = 63 beads). Lines are fits to Poisson distribution. (**h**) Activity of FL CENP-E relative to TR CENP-E in different assays (see Materials and Methods). Data are reported as Mean±SEM; n=24 independent experiments for bead assay, n=5 independent experiments for TIRF assay. Higher relative activity in the bead assay implies that FL CENP-E is more active when it carries a bead cargo than when it is bead-free.

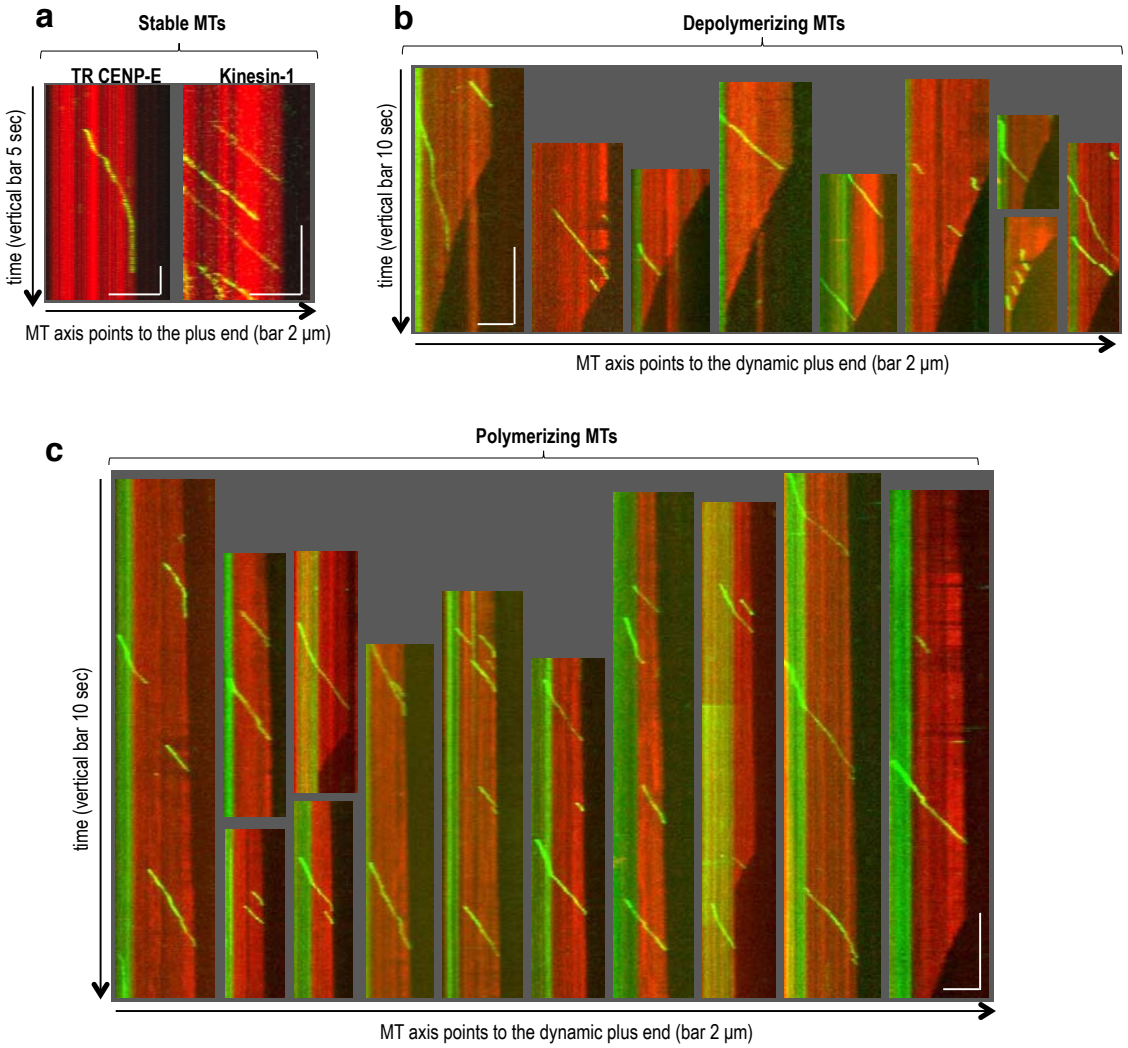

Figure S2 Transient association between TR CENP-E and the MT tips. Typical kymographs of TR CENP-E on MTs, observed with two-color TIRF. MTs are in red: HiLyte647 or dimly labeled Rhodamine tubulin was used. GFP-labeled motors are green. In some images the MT nucleating seeds are also green because they were grown using larger concentration of Rhodamine labeled tubulin, and excitation and imaging were carried out differently than with the HiLyte647 tubulin, see Materials and Methods. **(a)** TR CENP-E motor reaches and pauses shortly at the stable MT tip; under the same assay conditions the truncated kinesin-1 (K560-GFP) falls off without pausing, see text and Table S2 for more details. (**b**) TR CENP-E reaches and detaches quickly from the ends of depolymerizing MTs. (**c**) TR CENP-E reaches and detaches quickly from the ends of polymerizing MTs. In many of these kymographs the slope of CENP-E-GFP lines is less on red than on green MT segments, indicating that this motor walks slower on the GMPCPP-containing lattice (seeds) than on the GDP-containing MT walls (dynamic MT extensions).

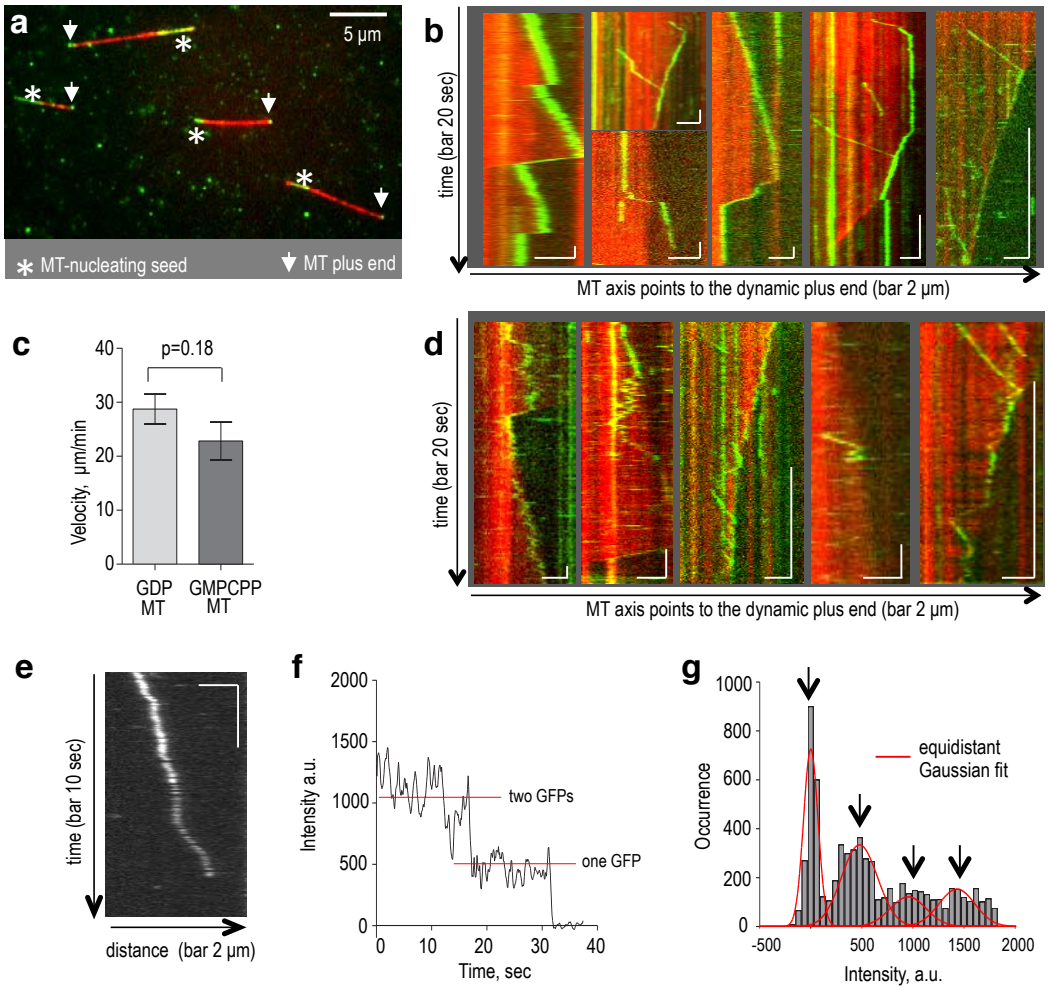

Figure S3 Lasting association between FL CENP-E and the dynamic MT tips. **(a)** The two-color TIRF microscopy image shows dynamic MT polymers (red) grown from the coverslip-attached seeds (in green, asterisks) in the presence of 4 nM GFP-labeled FL CENP-E (green). Decoration of the plus tips is evident (arrows). (**b**) Example kymographs of FL CENP-E complexes tracking the dynamic MT tips. The first panel shows a robust tracking by a bright dot, which contained 3-4 dimeric molecules (see also Video S7). All other images are for 1-2 dimeric motors. Last two panels correspond to Videos S5 and S4, respectively. (**c**) FL CENP-E velocity on the GMPCPP-containing MTs is slightly slower than on the GDP-MTs made with Taxol (unpaired t-test, n=18 molecules for each group). Data are Mean ± SEM (**d**) Kymographs showing the excursions of FL CENP-E away from the MT tip during the tracking. (**e**) A kymograph of a TR CENP-E motor molecule moving on Taxol-stabilized MT. The intensity of the moving dot changes in two steps, as seen from data in panel f. (**f**) Integral intensity (black line) of the moving TR CENP-E molecule shown in panel e. This curve was generated by smoothing the raw intensity data with a sliding average with window containing 7 data points, then subtracting the background. Red lines mark the intensity of 1 and 2 GFP molecules, as identified with the histogram on panel **g**. (**g**) Histogram of the intensity of GFP-labeled motors generated from the linescans, such as shown in panel **f**, for n=39 TR CENP-E molecules. Distance between two adjacent peaks (arrows) corresponds to the intensity of a single GFP molecule, see Materials and Methods.

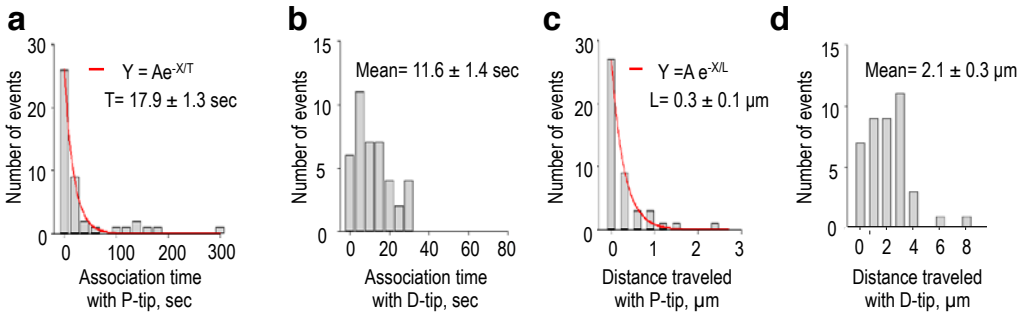

Figure S4 Quantification of the motility of FL CENP-E at dynamic MT tips (**a, b**) Histograms of the association time between FL CENP-E and the polymerizing (P, n = 45) and depolymerizing (D, n = 41) MT tips, respectively. (**c, d**) Histograms of the distances traveled by FL CENP-E with the P and D-tip, respectively. Errors in all panels represent SEM. Data from 8 independent experiments.

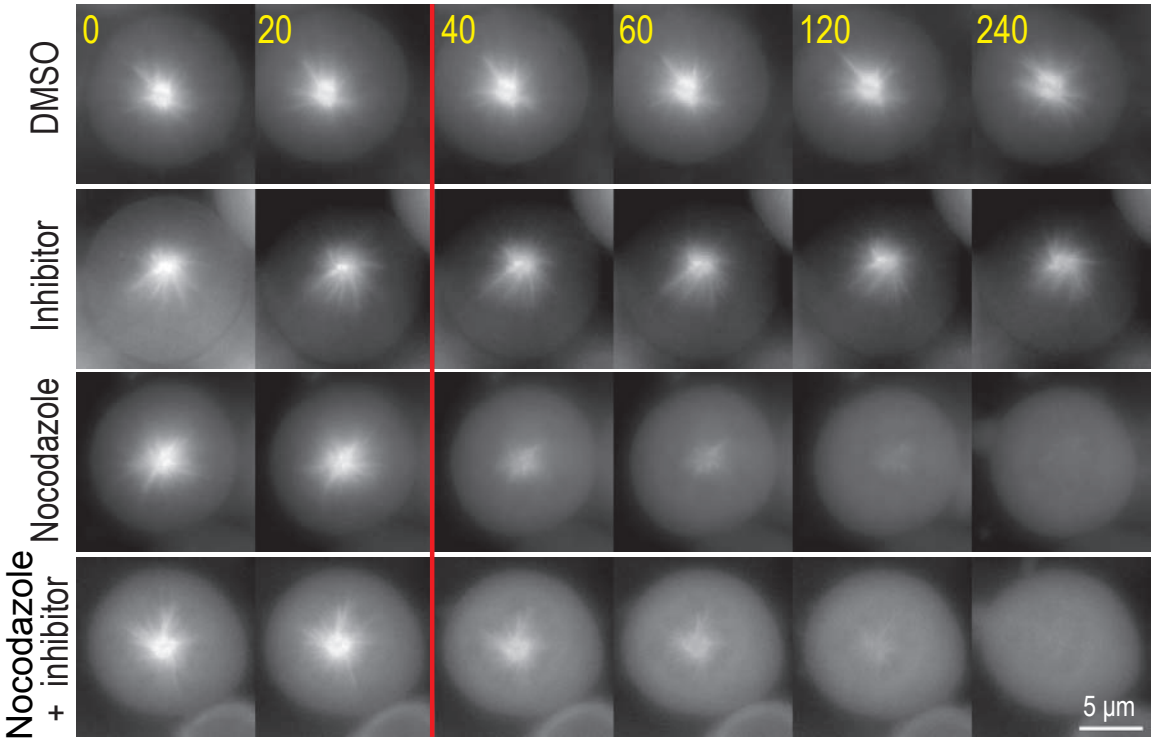

Figure S5 MT stability in monopolar spindles treated with different inhibitors. Representative images of HeLa cells treated as indicated, see Fig. 5b and main text for details. Numbers in yellow indicate time in seconds after the start of imaging. Red bar indicates the addition of drugs 20 sec after the start of imaging. The following number of cells were analyzed for each conditions; 50 cells for DMSO treated cell (control), 45 for CENP-E inhibitor treated cells, 50 for nocodazole treated cells and 40 cells were treated with both nocodazole and CENP-E inhibitor. Images were collected from 2 independent experiments. Nocodazole was used at 10 µM and CENP-E inhibitor (GSK-923295) at 200 nM.

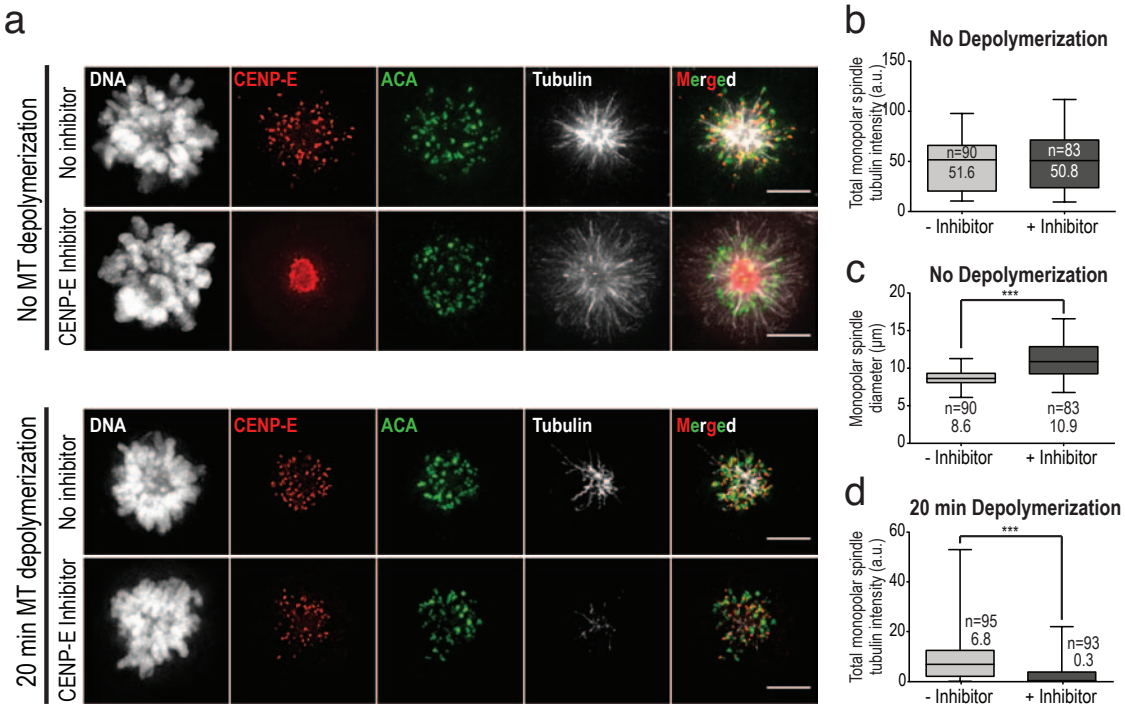

Figure S6 MT destabilization assay in cells with monopolar spindles. (**a**) Representative immunofluorescence images of monastrol-arrested HeLa cells with or without nocodazole treatment, which causes MT depolymerization. Prior to nocodazole application CENP-E was depleted from the kinetochores by adding GSK-923295. This removal occurs in the MT-dependent manner, consistent with induction of rigor CENP-E binding to kinetochore MTs and its subsequent passive transport to the spindle poles via poleward MT flux. DNA was visualized with H2B mCherry (white, left column), CENP-E was stained using HPX-1 anti CENP-E antibody (red), kinetochores were stained with anti-centromere antibodies (ACA, in green), and MTs were stained with anti-tubulin antibodies (DM1a, white, second from the right column). Merged images show a combination of ACA, CENP-E-GFP and tubulin signals. Scale bar here and on other panels is 5 µm. (**b**) Box and whiskers diagram shows total monopolar spindle tubulin intensity in the presence or absence of CENP-E inhibitor without nocodazole (no MT depolymerization); data are based on 90 cells for the control and 83 cells for the experimental condition (+ CENP-E inhibitor) acquired from 3 independent experiments. The two-tailed unpaired student t test indicates no significant differences between the two conditions. Here and in panels below, the lower bars in these boxes represent the first quartile values, the second and third quartile are represented by the plain box separated by the median (horizontal bar) and the value for fourth quartile is represented by the upper bars. (**c**) Box and whiskers diagram showing diameter of the monopolar spindles in the presence or absence of CENP-E inhibitor without nocodazole. Data are based on 90 cells for the control and 83 cells for the experimental condition (+CENP-E inhibitor) from 3 independent experiments. The two-tailed unpaired student t test indicates significant differences between the two conditions: *** $p < 0.001$. (**d**) Analogous quantification as in panel b but for cells in the presence or absence of CENP-E inhibitor 20 min after addition of nocodazole. Data are based on 95 cells for the control and 93 cells for the experimental condition (+CENP-E inhibitor) from 3 independent experiments. The two-tailed unpaired student t test indicates significant differences between the two conditions. *** $p < 0.001$.

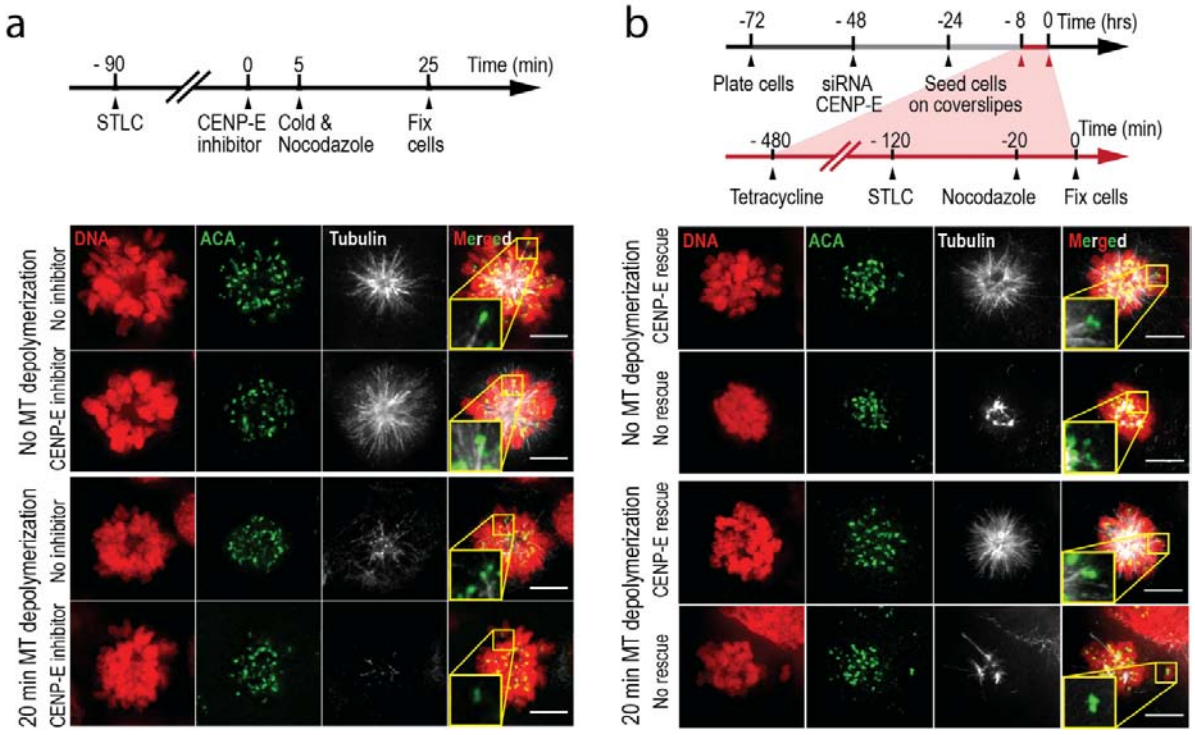

Figure S7 Reduced stability of kinetochore-MT attachments in two cell lines following CENP-E depletion from the kinetochores. (**a**) Timeline of the MT destabilization assay with monopolar spindles and representative images of fixed HeLa cells. Insets show two-color enlargements of the kinetochores on peripheral chromosomes (same images as in Fig. 5 panel e). See legend to Fig. 5 for details. Scale bar, 5 µm. (**b**) Schematics of the timing of RNAi and drug treatments (see Materials and Methods) and representative images of DLD-1 cells depleted of endogenous CENP-E and rescued (or not) with a GFP-tagged FL CENP-E. Insets show two-color enlarged images of the chromosomes (green) and MTs (white) at the periphery of the chromosome sphere. Similar results were obtained when CENP-E was depleted from the kinetochores with GSK-923295 or via RNAs approach.

Legends to Supplementary Tables

Supplementary Table S1. Interactions between CENP-E and MT lattice, as determined with single molecule TIRF and bead assays. Here and in other tables the numbers are Mean ± SEM, N, where N is the total number of observed events. For the beads assay only data from the microscopy chambers in which no more than 30% beads were motile are included. When bead motility is that infrequent, more than 80% of moving beads are likely to be driven by single motor molecules[53]. The velocity of single TR CENP-E molecules reported here is consistent with findings in[28,30] , but it is faster than in[6] due to the differences in assay conditions.

Supplementary Table S2. Interactions between CENP-E and MT tips. Data reported here were obtained with complexes containing 1-2 CENP-E dimers. The association time with stable tips was examined using Taxol-stabilized MTs. The association time and travel distance with polymerizing tips were determined from single exponential fits of the respective histograms (Fig. S4 panels a, c, red curves). The association time and travel distance with the depolymerizing tips (Fig. S4 panels b, d) and the association times with stable MT tips are reported as mean values. Time and distance of FL CENP-E motility with MT disassembly are likely to be underestimated because they were frequently limited by a short MT length. NA – not applicable.

Supplementary Table S3. Model parameters. Our mathematical model contains 11 independent parameters: 5 kinetic parameters to describe the rate of the transitions between different states, as illustrated in Fig. 7a, b, and 6 mechanical parameters. For further details about specifying the values of model parameters and model calibration see Mathematical Model of CENP-E Motility in Supplementary Note.

Legends to Supplementary Videos

Video S1. Loss of chromosome alignment in cells with inhibited CENP-E. HeLa cells expressing Tubulin-EYFP and Histone H2B-RFP (natural colors are inverted in this video for a better visualization) were released from the metaphase arrest in the presence (upper panel) or absence (lower panel) of CENP-E inhibitor GSK-923295 at the beginning of these sequences, played at 4 fps, 480 time faster than recorded. In bi-polar spindles with rigor-locked CENP-E several chromosomes lose their alignment and become stuck at the poles, leading to a prolonged cell cycle arrest.

Video S2. Truncated CENP-E carries a bead along Taxol-stabilized MT. At the start of this sequence, 0.5 μm bead coated with TR CENP-E is held with a weak optical trap near a coverslip-attached Taxol-stabilized MT. A piezo-stage is then repositioned to promote bead's contact with the MT. When the bead starts walking the trap is turned off to record the velocity and run length of bead motions. In such assays, the TR-coated beads moved similarly to the beads coated with FL CENP-E, demonstrating that the non-motor domains have little effect on CENP-E traditional transport along MT wall. Video was recorded in DIC at 7 fpse and 100 msec exposure; played 2 times faster than recorded. Scale bar 2 μm.

Video S3. Truncated CENP-E motors moving on a dynamic MT. Two TR CENP-E dimers sequentially land on the MT lattice and quickly walk to its growing plus end, where they detach readily. The MT then starts shortening, while another TR motor lands, walks and falls off the disassembling tip. Images were acquired with two-color TIRF, so the MT is dimmer towards the plus end where it is farther away from the coverslip. The coverslip-attached Rhodamine-labeled MT seed is green, because Rhodamine is excited with 488 nm laser. The 640 nm laser was used to visualize "red" Hilyte-647 tubulin. Time-lapse image sequence was acquired at 2 fps, played 5 times faster than recorded. Scale bar 2 μm.

Video S4. Motility of a full length CENP-E dimer on a disassembling MT. A single FL CENP-E dimer reaches and then tracks with a disassembling MT end, exhibiting processive motility in both plus- and minus- MT end directions. Motions were recorded as in Video S3 but continuously at 100 msec per channel, played 5 times faster than recorded. Scale bar 2 μm.

Video S5. Motility of full length CENP-E complexes on a dynamic MT. A FL CENP-E tetramer lands on MT lattice, reaches a growing tip and stays tip-associated during the phases of growth and shortening. Another FL CENP-E complex, likely a single dimer, joins the first complex, as it tracks with the disassembling end until both get stuck to the coverslip surface (see Fig. S3b left panel for the respective kymograph). Motions were recorded as in Video S4, played 3.3 times faster than recorded. Scale bar 2 μm.

Video S6. Motility of a full length CENP-E dimer on a growing MT. Arrow points to a single FL CENP-E dimer walking to a growing MT tip. Subsequently, the arrow's position is fixed; the GFP labeled protein continues to move slowly with MT polymerization, while displaying visible diffusion near the tip (see Fig. 8c for the respective kymograph). This sequence was recorded using only 488 nm laser, which excites both green and red fluorescence, subsequently separated via different emission. The coverslip-attached MT seed is seen as brighter red, due to a higher proportion of Rhodamine-labeled tubulin. Video is played 2 times faster than recorded. Scale bar 2 μm.

Video S7. Long-lasting association of full length CENP-E with a dynamic MT tip. A complex of 3-4 FL CENP-E dimers tracks a dynamic MT tip for several phases of MT growth and shortening. Motions were recorded as in Video S6; played 20 times faster than recorded. Scale bar 2 μm.

Video S8. Lack of coupling between beads coated with truncated CENP-E and depolymerizing MT end. Motor-coated bead (0.5 μm) walks to the plus-end of a MT, which was grown from a coverslip-attached axoneme and stabilized temporarily with a GMPCPP-containing, Rhodamine-labeled cap (arrowhead). With bright illumination, the Rhodamine-labeled MT cap is destroyed (images in red), triggering MT depolymerization and subsequent bead's detachment. Time-lapse images were acquired with low-light DIC, so individual MTs are hard to discern. Video was recorded at 1 fps with 60 msec exposure, played 7.5 times faster than recorded.

Video S9. Processive motion of the bead coated with full length CENP-E toward the plus, then minus MT ends. This video shows analogous experiment to that in Video S8 but with the bead coated with FL CENP-E. The bead is seen moving on the MT wall toward the plus-end of MT, but when the MT begins to shorten the bead moves in the minus-end direction in conjunction with MT disassembly. Arrow marks the initial position of the bead. Played 15 times faster than recorded.

Video S10. Live imaging of MT destabilization assay in cells with monopolar spindles. This video shows maximal projections of 3 confocal slices (0.5 μm/step) of HeLa cells expressing Mis12-GFP (kinetochore marker). Cells were treated with monastrol to create the mitotic configuration in which chromosomes are gathered in a rosette around the unseparated poles. MT depolymerization was induced by nocodazole at the beginning of these two sequences and motions of the kinetochores were recorded every 10 sec for 5 min. The inward chromosome motion is greatly reduced in the cell treated with CENP-E inhibitor. Video is played 150 times faster than recorded and repeated 3 times. Scale bar 5 μm.

Video S11. Computer model of the motility of full length CENP-E dimer on a growing MT. Motor domains are shown in blue and orange, CENP-E tails are pink and the coiled coil is grey. To simplify calculations, the motor walks along the same protofilament as the diffusing tail. Fluctuations in the length of MT protofilaments reflect fast tubulin exchange at the MT tip. This sequence shows the molecular events at a millisecond time scale, when MT elongation and motor's walking appear much slower relative to the tubulin exchange and the diffusion and binding/unbinding of the tail. Upon reaching the end of the protofilament track, the motor domains dissociate rapidly (with the rate of tubulin exchange) but remain tethered to the MT lattice via the diffusing tail. Tail's residency time on the MT lattice is 0.5 sec, while motor's re-binding to the lattice takes only 1 msec, so the motor is highly likely to resume the plus-end directed motion before the tail loses its MT association. Calculations were carried out with parameter values specified in Table S3 and with 20 μsec time step, only 1 out of every 50 frames is shown. Video is played at 10 fps, so 1 sec of the video corresponds to 10 msec of the 'model' time.

Video S12. Computer model of the motility of full length CENP-E dimer on a dynamic MT. This simulation is for a longer time than in Video S11, and it is played "faster" to show the relatively slow processes of MT elongation, shortening and CENP-E tip-tracking. For simplicity, the elongating and shortening MT ends were modeled similarly, but with different constants of tubulin exchange. CENP-E motor repeatedly walks to the end of the protofilament and detaches, but it remains tethered and quickly resumes its walking. This "tethered motor" tip-tracking mechanism requires both the motor and tail CENP-E domains, but it does not require that the CENP-E can discriminate between MT wall and its growing or shortening ends. The video was generated as Video S11, but only 1 out of every 2,500 frames is shown at 10 fps.

Mathematical Model of CENP-E Motility.

1. Model description.

CENP-E motility on MT wall. Our mathematical model of the motility of CENP-E dimer is based on the kinetic schemes shown in Fig. 7a,b. For simplicity, we considered only the MT-bound CENP-E molecules, and their soluble pool was not modeled. A single CENP-E molecule was assumed to contain 3 connected parts (*motor*, *tail* and *stalk*), each with distinct kinetic and stochastic properties. *Motor* moved in 8 nm steps to the plus MT end with the rate V_{motor} (see Table S3 for the list of all model parameters), and its detachment from the MT wall occurred with rate constant p_{motor}. The *tail* underwent one-dimensional diffusion with the diffusion coefficient D_{tail}, and dissociated from the MT wall with rate constant p_{tail}. These two domains were linked with the *stalk*, which was modeled as a worm-like chain (see below). Thus, the CENP-E molecule could attach to the MT wall either via its *motor* or *tail*, or both. When only the *motor* was MT-bound, *tail* binding occurred with rate constant $p_{reattach}$. Binding of the *motor* in a molecule that had the MT-bound *tail* also occurred with $p_{reattach}$. The CENP-E molecule could also become auto-inhibited with the rate constant p_{inhib}. The auto-inhibited molecule detached from the MT wall immediately (i.e. at the next calculation step).

MT dynamics. MT was modeled as a single protofilament, which elongated and shortened in 8 nm steps at one end (Fig. 7b). For simplicity, the protofilament was considered to be straight regardless of whether it was elongating or shortening. The kinetics of the protofilament polymerization were described with two parameters: the on-rate ($p_{on,PF}$) for tubulin binding to the end of the protofilament and the corresponding off-rate ($p_{off,PF}$). The latter parameter was not independent and was related to the velocity of the protofilament growth and the tubulin on-rate:

$$p_{off,PF} = p_{on,PF} - V_{PF\ growth}\ /l \qquad \text{(Eq. S1)}$$

Here l = 8 nm is the length of one tubulin dimer, $V_{PF\ growth}$ is the velocity of protofilament growth, and these rate constants correspond to MT growth. Depolymerization was described with analogous equation that takes into account that the net change in polymer's length is in the opposite direction than during polymerization and the rate constants correspond to MT shortening:

$$p_{off,PF} = p_{on,PF} + V_{PF\ shortening}\ /l \qquad \text{(Eq. S2)}$$

CENP-E interaction with dynamic MT tip. The *motor* that reached the tip of the stable MT detached from the terminal tubulin dimer with the rate constant p_{motor}, which was the same constant that described *motor's* dissociation from MT wall. At the dynamic MT end, the *motor* could also detach from the polymer concurrently with the dissociation of the terminal tubulin. Thus, the *motor's* detachment from the dynamic tip was given by the sum of two rates: $p_{motor} + p_{off,PF}$. Because the *motor*'s motility was unidirectional, the *motor* detachment from the dynamic MT tip was largely determined by the rate of tubulin exchange, which is much faster than the rate of spontaneous *motor's* dissociation defined by p_{motor} (see Table S3). Furthermore, since at the stable MT tip the rate of *motor's* detachment was determined only by p_{motor}, the in silico *motor* spent statistically longer time at the stable vs. dynamic MT tip, just as seen in the experiment (Table S2). Analogously, the rate of the *tail's* detachment from the dynamic MT tip, polymerizing or depolymerizing, was described by ($p_{tail} + p_{off,PF}$). If during the calculation the *tail* did

not dissociate from the MT tip, it was assumed to reverse the direction of its diffusive motion. This assumption is justified by our experimental observation that the majority of Tail molecules were "reflected" by the MT tip (Fig. 6 f-h). When the tail was modeled as described here, the frequency of its detachment from the dynamic tip in silico was similar to that determined experimentally. Importantly, the model had no additional assumptions about the differences in how these domains interacted with MT wall vs. tip structures; the interactions at the growing and shortening MT ends were also described identically.

2. Numerical calculations.

Computer simulations were carried out using a custom-made Matlab 2011b code (available by request) and with parameters specified in Table S3. To simplify calculations we assumed that the initial tail's binding was behind the *motor* heads, i.e. farther away from the MT tip. Binding of the *motor* in a molecule in which the *tail* was already bound to MT occurred in "front" of the *tail.* The relative positions and states ("attached" vs. "detached") of the *motor* head domains, *tail* and the MT tip were updated with 20 μsec calculation step. The CENP-E coordinates plotted on the simulated kymographs corresponded to the position of the *tail* (for FL CENP-E), or the *motor* domains (for TR CENP-E).

CENP-E stalk was represented with a worm-like chain generated as in[1] and using 115 segments with 2 nm length. TR CENP-E was modeled as FL CENP-E but using $p_{tail} = 10^4$, $p_{reattach} = 0$, such that the *tail* stayed detached from the MT during the course of simulations. FL CENP-E in the presence of AMPPNP or GSK923295 was modeled as FL CENP-E in the presence of ATP but with $V_{motor} = 0$, mimicking rigor binding to the MT wall. Additionally, after the depolymerizing MT tip reached the motionless *motor* and it dissociated together with the terminal tubulin subunit, the probability of this *motor*'s detachment from this subunit, and therefore the chance that it can re-attach to the MT wall, was zero, mimicking the irreversible binding between the *motor* and tubulin dimer in the presence of AMPPNP [2]. Qdot coated with TR CENP-E and CENP-E Tail was modeled similarly to FL CENP-E, except that the motor and tail domains were connected rigidly with 20 nm separation, the diameter of Qdots used in our experiments. Representative behavior of CENP-E in silico is shown in Figs. 7c-f and 8b-e, based on at least 10 simulations for each configuration. Residence times of different FL CENP-E proteins on MT wall and MT tips were calculated by running n=50 simulations for each configuration to determine the association times, then fitting the respective histograms with exponent. Theoretical data for "fast" and "slow" *tails* were calculated identically using the value of model parameters listed in Table S3, but the diffusion coefficient of the "slow" *tail* was 0.016 μm/s^2.

3. Choice of model parameters and model calibration (Table S3).

The value of parameters V_{motor} and D_{tail} were obtained from our experiments in vitro. The rate of MT growth ($V_{MT\ growth}$) and shortening ($V_{MT\ shortening}$) were measured based on kymographs of the dynamic MT ends in the absence of CENP-E tip-tracking using the same experimental chambers. Rate constants p_{motor} and p_{tail} are the reverse of the measured residence time (Table S1). Other parameters were specified as follows:

• $p_{reattach}$. The rate of *motor* and *tail* reattachment was estimated as inverse of the time it takes a globular protein to diffuse over the distance *L,* which corresponds to the contour length of CENP-E molecule:

$$p_{reattach} = 2D/L^2 = 2 \cdot 68\ \mu m^2 sec^{-1} / (0.23\ \mu m)^2 = 2.6 \cdot 10^3\ sec^{-1} \quad \text{(Eq.S3)}$$

where *D* is the diffusion coefficient of a globular protein in aqueous solution[3], L =230 nm (reference[4]).

• MT dynamics during polymerization. To estimate the on-rate of tubulin addition ($p_{on,PF}$) we used the reported value for the on-rate of MT elongation in 5 μM soluble tubulin (Fig. 6 E in reference[5]), which corresponds to tubulin concentration used in our two-color TIRF assays. Tubulin on-rate for individual protofilament $p_{on,PF}$ was calculated from this value by dividing it by the number of MT protofilaments: $p_{on,PF}$ = 266 sec^{-1}/13 = 20.5 sec^{-1}. The value of tubulin dissociation constant for the polymerizing ends $p_{off,PF}$ was calculated with Eq. S1, in which $V_{PF\ growth} = V_{MT\ growth}$, measured in μm/min units.

• MT dynamics during depolymerization. For the depolymerizing MT, the value of $p_{on,PF}$ was assumed to be negligible ($p_{on,PF} = 0$). The value of $p_{off,PF}$ was calculated using Eq. S2, in which $V_{PF\ shortening} = V_{MT\ shortening}$, measured in μm/min units.

• *P*. Persistence length of the stalk was estimated by building the distribution of head-to-tail distances $D_{H\text{-}T}$ of the electron microscopy images of FL CENP-E protein[4], then numerically solving the following equation[6]:

$$\langle {D_{H-T}}^2 \rangle = 2PL\left(1 - \frac{P}{L}\left(1 - e^{-\frac{P}{L}}\right)\right) \quad \text{(Eq. S4)}$$

where *L* is the contour length of CENP-E.

• To calibrate model we fitted the value of parameter p_{inhib}. The value of p_{inhib} was chosen such that the calculated residence time of the FL CENP-E on the MT lattice matched the experimentally measured value (Table S1).

Supplementary references

1. Nelson, P.C. *et al.* Tethered particle motion as a diagnostic of DNA tether length. *The journal of physical chemistry. B* **110**, 17260-17267 (2006).
2. Alonso, M.C. *et al.* An ATP gate controls tubulin binding by the tethered head of kinesin-1. *Science* **316**, 120-123 (2007).
3. Salmon, E.D., Saxton, W.M., Leslie, R.J., Karow, M.L. & McIntosh, J.R. Diffusion coefficient of fluorescein-labeled tubulin in the cytoplasm of embryonic cells of a sea urchin: video image analysis of fluorescence redistribution after photobleaching. *The Journal of cell biology* **99**, 2157- 2164 (1984).
4. Kim, Y., Heuser, J.E., Waterman, C.M. & Cleveland, D.W. CENP-E combines a slow, processive motor and a flexible coiled coil to produce an essential motile kinetochore tether. *The Journal of cell biology* **181**, 411-419 (2008).
5. Gardner, M.K. *et al.* Rapid microtubule self-assembly kinetics. *Cell* **146**, 582-592 (2011).

6. van Noort, J. *et al.* The coiled-coil of the human Rad50 DNA repair protein contains specific segments of increased flexibility. *Proceedings of the National Academy of Sciences of the United States of America* **100**, 7581-7586 (2003).